PALEOCEANOGRAPHY, VOL. 13, NO. 3, PAGES 225-244, JUNE 1998

Impact of oceanic reorganizations on the ocean carbon cycle and atmospheric carbon dioxide content

Olivier Marchal, Thomas F. Stocker, and Fortunat Joos

Climate and Environmental Physics, Physics Institute, University of Bern, Bern, Switzerland

Abstract. A zonally averaged, circulation-biogeochemical ocean model is used to explore how the distribution of PO_4 and $\delta^{13}C$ in the major basins and the atmospheric pCO_2 respond to rapid changes in the thermohaline circulation (THC). Different evolutions of the Atlantic THC are simulated by applying surface freshwater pulses typical, for example, of Heinrich events and the last deglaciation. In the model, when the THC completely collapses, PO_4 increases (>0.5 mmol m^{-3}) and $\delta^{13}C$ decreases (<0.5 ‰) in Atlantic bottom waters because of a drop in ventilation by North Atlantic Deep Water (NADW). Although consistent with the traditional interpretation of sedimentary records of benthic foraminiferal Cd/Ca and $\delta^{13}C$, the relationship between the degree of PO_4 enrichment and $\delta^{13}C$ depletion and the degree of THC reduction is not linear. In the NADW formation area the preformed PO_4 declines (<0.5 mmol m^{-3}) because of an imbalance between biological uptake and PO_4 supply from the deep, and the preformed $\delta^{13}C$ rises (>1‰) because of a longer residence time of waters at the surface. These surface anomalies are propagated to the bottom North Atlantic when the THC resumes. When the thermohaline overturning is only partly reduced and at shallower depths, changes in bottom waters are accompanied by a PO_4 decrease and $\delta^{13}C$ increase at intermediate levels in the mid-latitude Atlantic. This results in enhanced vertical gradients of these properties consistent with chemical and isotopic reconstructions for the last glacial maximum. Finally, the atmospheric pCO_2 increases during the cold period in the North Atlantic when the THC is reduced with an amplitude (7–30 μatm) and timescale ($\sim 10^2$ to 1–2 $\times$ 10^3 yr) depending on the intensity of the THC change. This is qualitatively consistent with recent data from an Antarctic ice core documenting a pCO_2 increase during the Younger Dryas and after Heinrich events 4 and 5.

1. Introduction

High-resolution analyses of deep-sea sediment and polar ice cores document a large variability of climate proxies at suborbital timescales during the last glacial period. Deep-sea cores raised from the North Atlantic revealed the presence of layers with an unusually high percentage of lithic fragments in the coarse size fraction [*Heinrich*, 1988; *Broecker et al.*, 1992; *Bond et al.*, 1992]. Six of these "Heinrich layers" were deposited at about 5–15 kyr intervals between marine stage boundaries 1/2 (12 ka B.P.) and 4/5 (74 ka B.P.) [*Bond et al.*, 1992; *Bond et al.*, 1993]. Heinrich deposits result from short-lived and massive discharges of icebergs originating from ice sheets in the northern hemisphere, and their presence between 40° and 55°N in the Atlantic indicates extremely low sea surface temperatures [*Bond et al.*, 1992]. Large and abrupt oscillations of $\delta^{18}O$ were found, on the other hand, in Greenland ice cores during the last glacial period [*Dansgaard et al.*, 1982; *Oeschger et al.*, 1984]. About 15 of these "Dansgaard-Oeschger" (D-O) events, occurring apparently at irregular intervals, were identified during marine stage 3 (i.e., between 24–59 ka B.P.) [*Johnsen et al.*, 1992; *Dansgaard et al.*, 1993]. They, too, are associated with the occurrence of ice-rafted debris in North Atlantic sediments [*Bond and Lotti*, 1995]. On the basis of the present geographic relationship between $\delta^{18}O$ of precipitation and air temperature at polar sites the D-O interstadials provide evidence of large shifts in temperature over Greenland, reaching on average an amplitude of ~7°C [*Johnsen et al.*, 1992] or perhaps even more [*Johnsen et al.*, 1995]. The last prominent change of $\delta^{18}O$ in Greenland ice cores is associated with the Younger Dryas cold event [*Dansgaard et al.*, 1989] that brought the North Atlantic region back to near-glacial conditions between ~12–13 ka B.P.

Because the intervals between Heinrich and D-O events are shorter than Milankovitch periodicities, feedback mechanisms internal to the glacial climate system are commonly invoked to explain their occurrence in the paleoclimatic record. Abrupt changes in the ocean thermohaline circulation (THC) constitute a paradigm in this regard because of the strong influence of the THC on the climate of the high northern latitudes today [*Broecker*, 1991] and given observational [e.g., *Boyle and Keigwin*, 1982; *Curry et al.*, 1988] and the-

Paper number 98PA00726.
0883-8305/98/98PA-00726$12.00

oretical evidence [e.g., *Stommel*, 1961; *Bryan*, 1986] that the THC can exhibit quite different modes. Periodic discharges of freshwater into the ocean arising from the partial disintegration of ice sheets are a prime candidate to produce abrupt thermohaline variability and hence both D-O and Heinrich cycles [*Broecker et al.*, 1990; *Paillard and Labeyrie*, 1994]. Recently, several model studies attempted to identify the impact of freshwater discharges on regional and global climates [*Maier-Reimer and Mikolajewicz*, 1989; *Wright and Stocker*, 1993; *Rahmstorf*, 1995; *Manabe and Stouffer*, 1995; *Schiller et al.*, 1997; *Manabe and Stouffer*, 1997; *Fanning and Weaver*, 1997; *Mikolajewicz et al.*, 1997; *Fawcett et al.*, 1997] and on the distribution of $\Delta^{14}C$ and $\delta^{18}O$ in the oceans [*Lehman et al.*, 1993; *Stocker and Wright*, 1996; *Mikolajewicz*, 1996].

In this paper, we use a zonally averaged, circulation-biogeochemical ocean model to explore quantitatively the impact of fast THC changes on the large-scale distribution of PO_4 and $\delta^{13}C$ in the major ocean basins and on the atmospheric pCO_2. This study is motivated by the significant suborbital variability exhibited by the proxies of these three variables during the last glacial period. For instance, recent $\delta^{13}C$ measurements on foraminiferal shells in several cores from the North Atlantic indicate that Heinrich events were accompanied by a drastic decrease in deep water $\delta^{13}C$ in this basin [*Vidal et al.*, 1997]. CO_2 measurements in the Byrd ice core (West Antarctica) suggest, on the other hand, that the atmospheric pCO_2 has increased during the Younger Dryas [*Blunier et al.*, 1997] and after Heinrich events 4 and 5 [*Stauffer et al.*, 1998].

The paper is organized as follows. In section 2 the steady state of the model is briefly described. This model captures the major features in the observed large-scale distribution of biogeochemical tracers in the modern oceans [*Marchal et al.*, 1998] and is a useful compromise for paleoclimate studies between box models (which lack any description of the ocean dynamics) and three-dimensional (3D) models (which are computationally expensive so that the duration of the integrations and the number of sensitivity experiments are severely limited). In section 3 we examine the changes in the latitude-depth distribution of PO_4 and $\delta^{13}C$ and in the atmospheric pCO_2 arising from a freshwater discharge. In section 4, sensitivity experiments are conducted. Finally, in section 5 the relevance of our model simulations in the light of the fast variability documented in deep-sea and polar ice records for the last glacial period is discussed.

2. Model Description

2.1. Physical Components

The model includes three physical components, namely, the zonally averaged ocean circulation model of *Wright and Stocker* [1992], the 1D energy balance model of the atmosphere of *Stocker et al.* [1992a] and the thermodynamic sea ice model described by *Wright and Stocker* [1993]. The coupling between these different components allows shifts between different climate states when perturbing the THC [*Stocker et al.*, 1992a; *Wright and Stocker*, 1993]. In the ocean the Atlantic, Indian, and Pacific are represented separately and connected in the south by a circumpolar channel. The circulation parameters [*Marchal et al.*, 1998, Table 1] produce distributions of temperature, salinity, and $\Delta^{14}C$ that are consistent with data in the modern oceans. The atmosphere, on the other hand, is zonally averaged and represented by one vertical layer. The atmosphere and sea ice parameters are listed in Table 1 of *Wright and Stocker* [1993].

2.2. Biogeochemical Components

The model simulates the transfer of total carbon ($\equiv {}^{12}C + {}^{13}C$) and ^{13}C between the rapidly exchanging carbon reservoirs of the ocean, the atmosphere and the land biosphere. River input and sediment burial are not included; that is, all the organic C and $CaCO_3$ produced in the ocean euphotic zone are recycled in the underlying water column. The cycles of organic C and $CaCO_3$ in the ocean are described using the biogeochemical model of *Marchal et al.* [1998]. For the chosen parameter values (Table 1) the model produces realistic distributions of phosphate, apparent oxygen utilization, total dissolved inorganic carbon (DIC), alkalinity and $\delta^{13}C$ of DIC compared with data in the modern oceans. The mass balance equations for total C and ^{13}C in the atmosphere and land biosphere are given in the appendix. Briefly, the atmosphere is considered as a well-mixed reservoir with respect to total C ($\equiv {}^{12}CO_2 + {}^{13}CO_2$) and ^{13}C ($\equiv {}^{13}CO_2$). The land biosphere, on the other hand, consists of four different carbon pools [*Siegenthaler and Oeschger*, 1987]. Because we focus on direct biogeochemical impacts of THC changes in the ocean and the atmosphere, possible variations in the terrestrial biomass and productivity arising from climate changes are neglected. The land biosphere, however, is included as a model component in order to account for the effect of terrestrial carbon fluxes in diluting ocean-mediated perturbations in atmospheric $\delta^{13}C$.

2.3. Initial Steady State

We describe below the five-step procedure for producing a model steady state suitable for freshwater input experiments. At each step a physical or chemical constraint on the ocean-atmosphere system is relaxed. In step 1 (10 kyr of integration) the model is spun up by restoring temperature T and salinities S in the surface layer (top 50 m) and PO_4 in the euphotic zone (top 100 m) to the observed zonal averages in the modern oceans

Table 1. Parameters of the Ocean Biogeochemical Model

	Definition	Value	Units	Reference
z_{eup}	depth of the euphotic zone	100	m	
τ_{PO_4}	relaxation time for euphotic zone PO_4	100	d	
K_{PO_4}	half-saturation constant for PO_4 uptake	0.4	mmol m^{-3}	*Nalewajko and Lean* [1980]
ϵ	exponent in fast-sinking POC [a] remineralization profile	0.858	1	*Bishop* [1989]
σ	fraction of reduced C in DOC_l [b]	0.5	1	
$\overline{DOC_l}$	ocean mean content of DOC_l	10	mmol m^{-3}	
κ	decay rate of DOC_l	variable	d^{-1}	
$\overline{r_p}$	ocean mean C_{CaCO_3}:C_{org} production ratio	0.06	mol mol^{-1}	
L_{dis}	length scale for $CaCO_3$ dissolution	3000	m	
α_{org}	fractionation factor for photosynthesis	variable	1	*Rau et al.* [1989]
α_{car}	fractionation factor for calcification	1	1	*Mook* [1986]
μ	air-sea CO_2 transfer coefficient	0.067	mol m^{-2} μatm^{-1}	*Broecker et al.* [1985]
Redfield ratios				
C:P		117	mol mol^{-1}	*Anderson and Sarmiento* [1994]
N:P		16	mol mol^{-1}	*Anderson and Sarmiento* [1994]
O_2:P	for O_2 consumption	-170	mol mol^{-1}	*Anderson and Sarmiento* [1994]
O_2:P	for O_2 production	variable	mol mol^{-1}	*Anderson and Sarmiento* [1995]

[a]Particulate organic carbon.
[b]Biologically labile dissolved organic carbon.

(see details given by *Marchal et al.*, 1998). Restoring fluxes are calculated as

$$J(\mathcal{T}) = \frac{\mathcal{T} - \mathcal{T}_r}{\tau(\mathcal{T})} \quad (1)$$

where $\mathcal{T} \in \{T, S, PO_4\}$, $\mathcal{T}_r$ is the local restoring value, and τ is a restoring time. $J(PO_4)$ is considered equivalent to the new production (here in P units) with $J(PO_4) = 0$ when $PO_4 < PO_{4,r}$ [*Najjar et al.*, 1992]. The rates of net production of all the other biogeochemical tracers are then related stoichiometrically to $J(PO_4)$. In step 1 we prescribe a preindustrial atmospheric $pCO_2 = 280$ μatm [*Neftel et al.*, 1988] and $\delta^{13}C = -6.5‰$ [*Leuenberger et al.*, 1992]. At the end of step 1 we diagnose the steady state values of PO_4 and $J(PO_4)$ in the euphotic zone ($PO_{4,d}$ and $J_d(PO_4)$, respectively). These values are then introduced in step 2 (1 kyr) into a Michaelis-Menten equation to describe new production as a function of PO_4 availability in the euphotic zone:

$$J(PO_4) = J_{pot}(PO_4)\frac{PO_4}{K_{PO_4} + PO_4} \quad (2a)$$

where

$$J_{pot}(PO_4) = J_d(PO_4)\frac{K_{PO_4} + PO_{4,d}}{PO_{4,d}} \quad (2b)$$

K_{PO_4} is a half-saturation constant for PO_4 uptake and $J_{pot}(PO_4)$ is a "potential" new production that would be achieved if $PO_4 \gg K_{PO_4}$. Equation (2a) is a simple parameterization allowing for changes in biological cycling due to changes in surface nutrient concentration when the ocean circulation is altered [*Siegenthaler and Wenk*, 1984]. In step 3 (1 kyr) the atmospheric pCO_2 and $\delta^{13}C$ are then allowed to evolve freely according to the exchanges with the ocean surface and with the land biosphere. In step 4 (1 kyr) we switch from restoring to mixed boundary conditions; that is, sea surface T are still restored to present-day observations, but the salt fluxes diagnosed from restoring are kept constant. Finally, in step 5 (7 kyr) the ocean model is coupled to the atmospheric energy balance and thermodynamic sea ice models. All model outputs remain virtually unchanged after step 1.

In the final model steady state the Atlantic is characterized by the injection of PO_4-depleted and $\delta^{13}C$-rich waters in the north due to the formation of North Atlantic Deep Water (NADW) (Figures 1a–2a). In the other basins, PO_4 increases and $\delta^{13}C$ decreases from south to north in the bottom waters, with PO_4 and $\delta^{13}C$ extrema located in the intermediate waters. These large-scale features are consistent with data in the modern oceans. Discrepancies compared to these data, on the other hand, are too low $\delta^{13}C$ in the deep Atlantic and too large $\delta^{13}C$ in the deep Indian and Pacific [*Marchal et al.*, 1998].

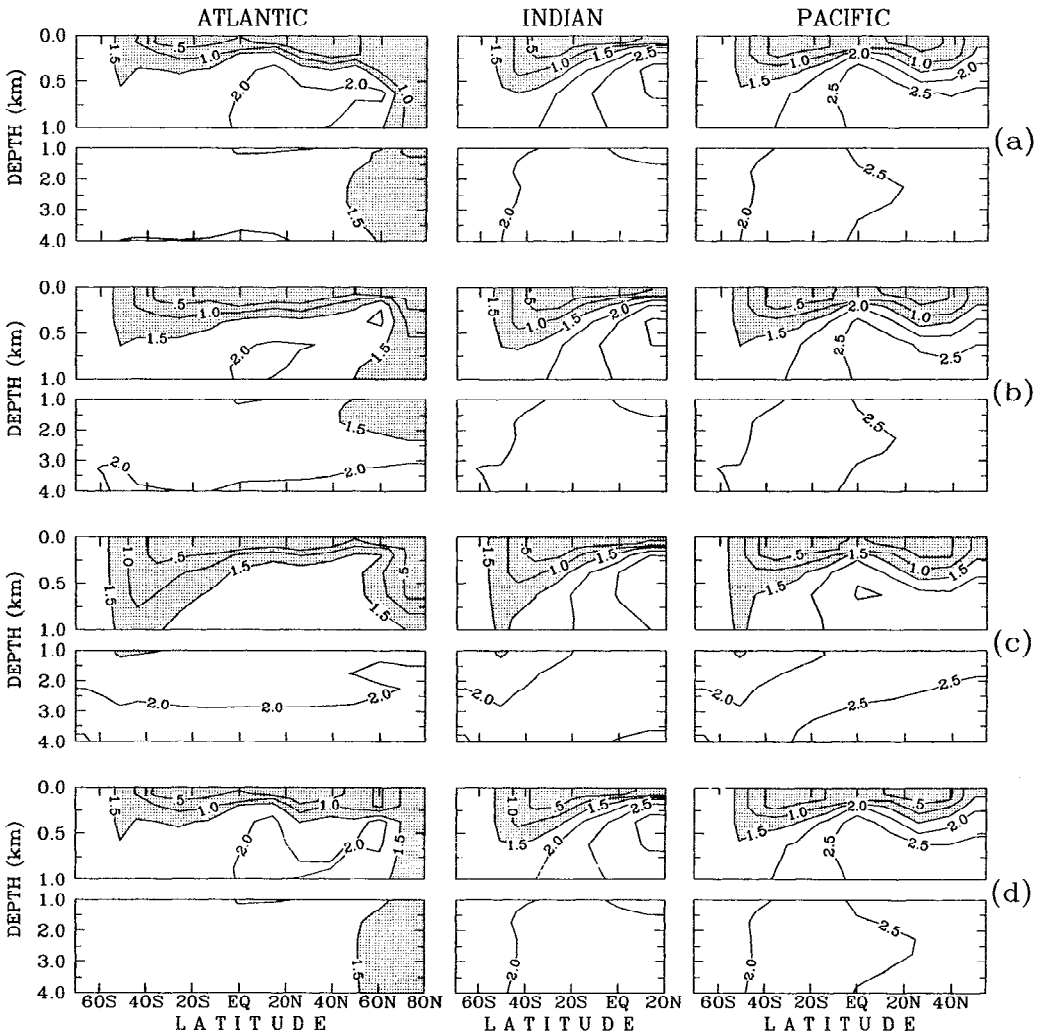

Figure 1. Latitude-depth distributions of PO_4 (mmol m^{-3}) in the reference simulation at (a) t = 1 ka (initial steady state; start of freshwater inputs (FI)); (b) 1.4 ka; (c) 2 ka (end of FI); and (d) 4.8 ka. Regions where PO_4 < 1.5 mmol m^{-3} are dashed. The contour interval is 0.5 mmol m^{-3}.

2.4. Applied Freshwater Inputs

We now examine the response of the model to "triangular" freshwater inputs (FI), with the rate of FI increase equal to the rate of subsequent FI decrease [*Mikolajewicz et al.*, 1997]. With this assumption the evolution of the FI is fully constrained by two quantities: the total volume of freshwater discharged, V (or equivalently the maximum FI), and the duration of the FI, D. From shifts in planktonic foraminiferal $\delta^{18}O$ identified in several deep-sea cores, *Labeyrie et al.* [1995] estimated that $\sim 10^6$ km^3 of ice were introduced into the North Atlantic during each Heinrich event. This volume is 1 order of magnitude lower than estimates of 9×10^6–10^7 km^3 for the two meltwater pulses of the last deglaciation, MWP-1A and MWP-1B, recorded in Barbados corals (from sea level changes of 24–28 m given by *Fairbanks* [1989]). According to ^{14}C datings on foraminiferal shells sampled at the top and bottom of Heinrich layers in two North Atlantic cores, Heinrich events lasted between 0.77 and 2.2 kyr [*Vidal et al.*, 1997, Table 1]. Coral-based sea level records, on the other hand, indicate durations of ~0.5–2 kyr for MWP-1A and MWP-1B [*Fairbanks*, 1990; *Edwards et al.*, 1993; *Bard et al.*, 1996]. To cover the broad range of observational estimates of V and D, we vary V from 0.5 $\times$ 10^6 to 10^7 km^3 and D from 0.25 to 2.5 kyr in our FI experiments.

In addition to its volume and duration the geographic location and chemical composition of the FI must also be specified. Analyses of deep-sea sediments indicate that icebergs have melted in the North Atlantic between 40° and 55°N during Heinrich events [*Bond et al.*,

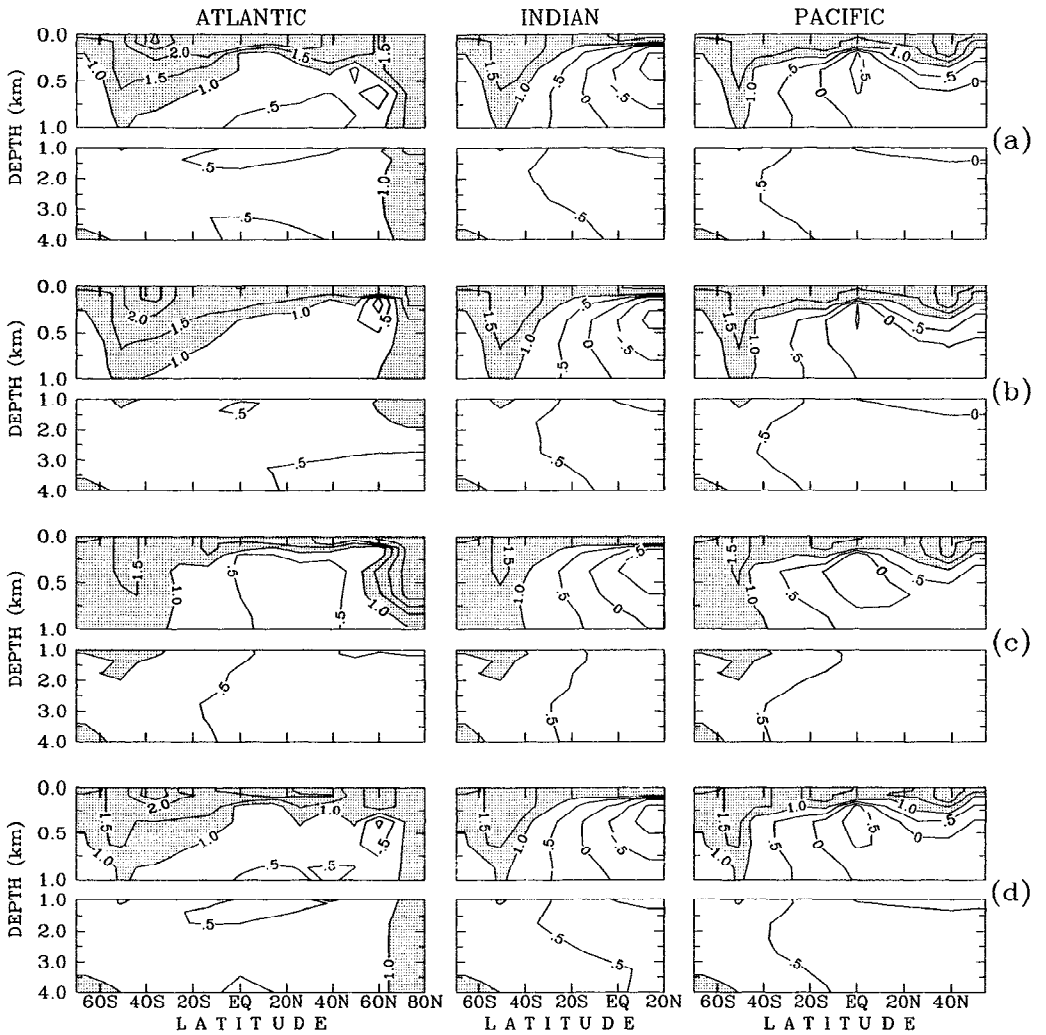

Figure 2. Latitude-depth distributions of $\delta^{13}C$ (‰) in the reference simulation at (a) $t = 1$ ka (initial steady state; start of FI); (b) 1.4 ka; (c) 2 ka (end of FI); and (d) 4.8 ka. Regions where $\delta^{13}C > 1$‰ are dashed. The contour interval is 0.5‰.

1992; *Grousset et al.*, 1993]. The locations of FI associated with MWP-1A and MWP-1B are more uncertain, as both pulses could have resulted, at least partly, from melting of the Antarctic ice sheet [e.g. *Clark et al.*, 1996]. Here we examine model results when FI is applied into distinct latitudinal bands where meltwater was likely discharged for the last glacial period and the last deglaciation. These bands are located in the Atlantic between 20° and 32.5°N (including the Gulf of Mexico), 32.5° and 45°N, and 45° and 55°N (St. Lawrence estuary) and along the Antarctic perimeter between 70° and 62.5°S. With regard to the chemical composition of the FI we assume that freshwater does not contain any of the chemical species which are simulated in the ocean model (i.e., the dilution effect of the FI will be maximum). For those species contributing to DIC and alkalinity in seawater (ALK) this is justified by the fact that glacial ice from Greenland and Antarctica has a low content of total inorganic carbon (between ~1–10 mmol m^{-3} [*Neftel et al.*, 1982]) and organic species (< 1 mmol m^{-3} [*Legrand and Mayewski*, 1997]). Concerning pCO_2 changes driven by dissolution only we note that the effects of DIC and ALK changes on seawater pCO_2 cancel out almost completely [*Takahashi et al.*, 1993].

3. Freshwater Experiments

3.1. Physical Response

In all FI experiments the rates of evaporation E, precipitation P, and (background) runoff R are kept constant in each latitudinal cell of the model. The surface water balance is thus altered only in that cell receiving the prescribed FI. Using the same model as ours, *Wright*

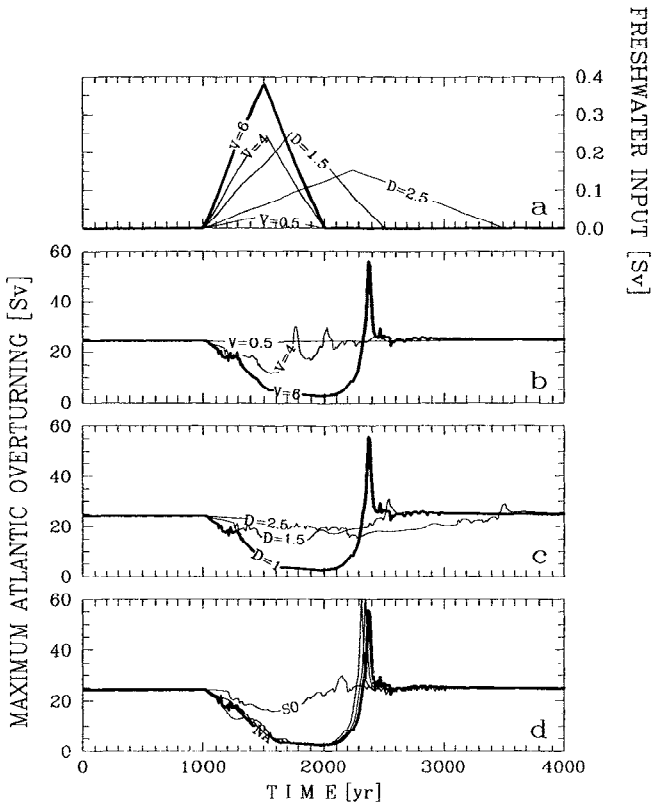

Figure 3. Evolution of (a) FI and (b–d) maximum zonal mean stream functions below 750 m in the Atlantic (Ψ_{max}). In the reference simulation (thick solid lines), total discharged volume V is 6×10^6 km^3; FI duration D is 1 kyr; and the FI is applied in the Atlantic between 32.5° and 45°N. Volume, duration, or geographic application of the FI has been varied as indicated in a series of sensitivity analyses. In Figure 3d, NA and SO are model results when FI is applied in the different latitudinal bands in the North Atlantic (20°–32.5°N, 32.5°–45°N, and 45°–55°N) and along the Antarctic perimeter (70°–62.5°S) in the Southern Ocean, respectively.

and Stocker [1993] and *Stocker and Wright* [1996] reduced the runoff into the northern North Atlantic in order for the ocean thermohaline circulation in the Atlantic to resume after the FI. This "runoff adjustment" is not included in our simulations, for the THC recovers spontaneously without changing the field of $E-P-R$. This is due to the fact that the fields of $E-P-R$, which we diagnose when switching from restoring to mixed boundary conditions and which influence the stability of the THC, are different from those diagnosed in previous studies (because of slightly changed circulation parameters). The transient behavior of the circulation itself, timescales, and amplitudes of property changes are, however, not sensitive to this modification.

Figure 3a displays prescribed freshwater inputs for various values of V and D. The corresponding changes in the maximum (zonal mean) stream function in the Atlantic below the region affected by wind, Ψ_{max}, are shown in Figures 3b–3c (when FI is applied between 32.5° and 45°N in the Atlantic). Within the range of V and D values considered the response of thermohaline circulation varies from only minor changes (5%

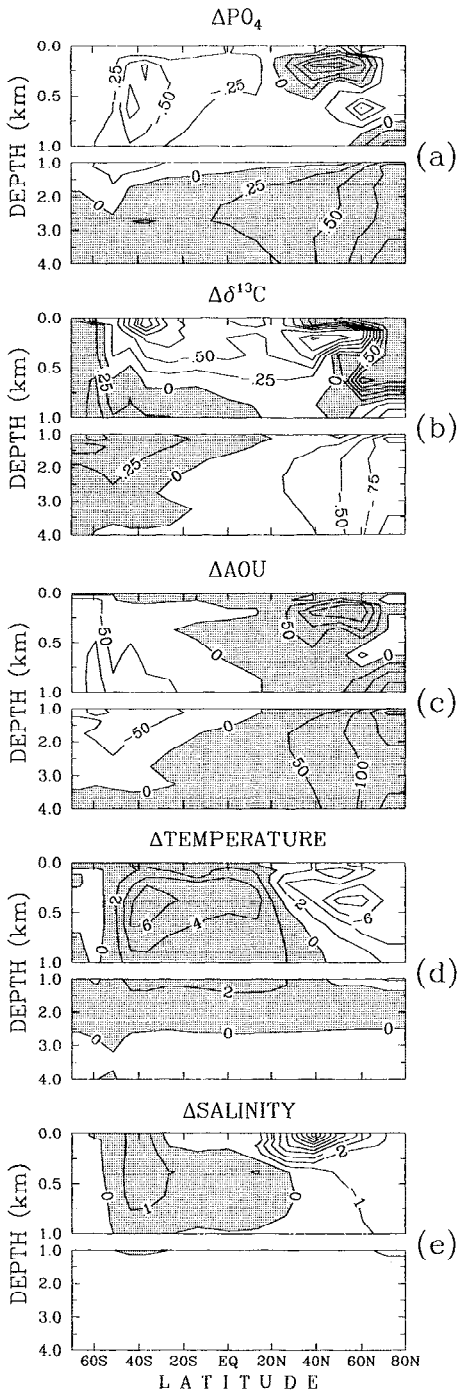

Figure 4. Latitude-depth distributions in the Atlantic of different anomalies between $t = 1$ ka (start of FI) and 2 ka (end of FI) in the reference simulation: (a) PO_4 (mmol m^{-3}), (b) $\delta^{13}C$ (‰), (c) apparent O_2 utilization (AOU) (mmol m^{-3}), (d) temperature (°C), and (e) salinity. Regions where changes are positive are dashed. The contour intervals are 0.25 mmol m^{-3}, 0.25‰, 50 mmol m^{-3}, 2°C, and 1.

with $V = 0.5 \times 10^6$ km^3 and $D = 1$ kyr) to a drop of 1 order of magnitude of the overturning rate in the Atlantic (with $V = 6 \times 10^6$ km^3 and $D = 1$ kyr). The reduction of Ψ_{max} is larger for a greater volume of freshwater discharged and for a shorter duration of the FI. This indicates that the time rate of change of the FI is a crucial parameter in the transient simulations. In the model the changes in Ψ_{max} are, indeed, related to a competition between the buildup of a freshwater cap in the North Atlantic and its removal by the ocean circulation and surface evaporation [*Wright and Stocker*, 1993]. Ψ_{max} changes are very similar when the freshwater is introduced into the different latitudinal bands of the North Atlantic (Figure 3d). On the other hand, the circulation response is much less when the freshwater is discharged along the Antarctic perimeter, as expected (reduction of 35% of Ψ_{max} with $V = 6 \times 10^6$ km^3 and $D = 1$ kyr).

The overturning rate exhibits an "overshoot" in the simulations with a large reduction in the Atlantic THC (at 2.3–2.4 ka in Figures 3b–3c). Then the initial overturning rate is always recovered after the freshening event although low salinity water is still found in one grid cell in the North Atlantic at the new steady state (Figures 3b–3c; see also *Wright and Stocker* [1993, Figure 9]). The overshooting was observed in previous freshwater experiments with the same model [*Stocker and Wright*, 1996] and a 3D model [*Mikolajewicz and Maier-Reimer*, 1994]. It is due in our model to a positive feedback when the THC resumes [*Wright and Stocker*, 1991]. When Ψ_{max} reaches the minimum, deep waters in the northern North Atlantic are warmer and more saline than surface waters (Figures 4d–4e; see also *Stocker and Wright* [1996, Figures 5c–5d]). When the surface freshwater cap is gradually eroded, stratification weakens until convection is initiated. This brings warm and saline waters to the surface. Excess heat is rapidly lost to the atmosphere resulting in further buoyancy loss. This positive feedback amplifies the convective activity and the associated overturning rate in the North Atlantic.

Next we analyze biogeochemical impacts in the ocean and the atmosphere of a reference perturbation where FI is applied between 32.5° and 45°N in the Atlantic with $V = 6 \times 10^6$ km^3 and $D = 1$ kyr (thick solid line in Figure 3).

3.2. Changes in the Oceanic Distributions of PO_4 and $\delta^{13}C$

The major anomalies in PO_4 (Figures 1b–1d) and in $\delta^{13}C$ (Figures 2b–2d) are found in the Atlantic where strong vertical gradients in PO_4 and $\delta^{13}C$ develop in the north (note, however, that PO_4 in the deep Pacific is slightly reduced at the end of the FI). About 3 kyr after the end of the FI the initial distributions of PO_4 and $\delta^{13}C$ are almost recovered; that is, waters with low PO_4 and high $\delta^{13}C$ are again reaching the ocean bottom in the North Atlantic. Below we consider two major anomalies that may have strong paleoceanographic implications (Figures 4a–4b). The first is the PO_4 increase and $\delta^{13}C$ decrease in the bottom waters, where $\Delta PO_4 > 1$ mmol m^{-3} and $\Delta\delta^{13}C < 1$‰ in the northern North Atlantic. The second is the large negative $\Delta PO_4 < 0.5$ mmol m^{-3} and positive $\Delta\delta^{13}C > 1$‰ in the upper water column in the same region.

3.2.1. PO_4 enrichment and $\delta^{13}C$ depletion in the bottom Atlantic. The tracer anomalies in the deep ocean can be related to changes in the distribution of water masses, in the distribution of preformed (i.e., surface) PO_4 and $\delta^{13}C$, and/or in the production of PO_4 and $\delta^{13}C$ at depth because of the oxidation of organic matter ($\delta^{13}C$ is not affected by the cycle of $CaCO_3$ in our model [*Marchal et al.*, 1998]). We show below that the PO_4 and $\delta^{13}C$ anomalies in the bottom Atlantic are due to a reduced ventilation by newly formed NADW.

The maximum PO_4 and $\delta^{13}C$ anomalies simulated in the bottom waters of the North Atlantic are almost proportional to each other (Figures 4a–4b). The proportionality factor, ~ -1 ‰ (mmol m^{-3})$^{-1}$, is similar to that expected if only organic matter cycling is taking place [*Broecker and Maier-Reimer*, 1992] and points to the oxidation of organic matter as an instrumental process in producing these anomalies. In order to test this hypothesis we inspect the changes in the latitude-depth distribution of the apparent O_2 utilization (AOU) (Figure 4c). Changes in AOU are mostly indicative of changes in the balance of the rates of oxidation versus ventilation because the surface AOU (= 0 mmol m^{-3}) is constant in our model. Compared to the initial steady state, AOU in the deep Atlantic is much larger when the THC is collapsed (Figure 4c). The AOU increase is up to 150 mmol m^{-3} in the bottom water in the northernmost part of this basin. A respiratory AOU increase of 150 mmol m^{-3} is accompanied by a PO_4 increase of $\sim$0.9 mmol m^{-3} and a $\delta^{13}C$ decrease of ~ 1.0‰ based on model stoichiometry only (Table 1). This is comparable to the simulated PO_4 and $\delta^{13}C$ anomalies.

PO_4 and $\delta^{13}C$ anomalies simulated in the bottom Atlantic are not related to an increase in new production that would, in turn, increase the oxidation rate of organic matter at depth. In the model the carbon that is reduced during new production in the euphotic zone is partitioned between fast sinking particulate organic carbon (POC) and labile dissolved organic carbon (DOC_l). The fast sinking POC that is produced is remineralized instantaneously in the underlying aphotic zone (below 100 m) according to a profile consistent with sediment trap data. By contrast, DOC_l is transported explicitly by the ocean circulation and remineralized below 100 m assuming first-order kinetics [*Marchal et al.*, 1998] (see also Table 1). The new production in the whole Atlantic (between 70° and 80°N) drops until the maximum FI

to 60% of its initial value. Then it increases slightly to only 70% of this value at $t = 2$ ka (short dashed line in Figure 5a). The decrease in new production is due to an increasing stabilization of the water column by freshwater capping which inhibits the recharge of PO_4 from the deep. The subsequent increase is associated, on the other hand, with the removal of the freshwater cap. Thus the PO_4 and $\delta^{13}C$ anomalies in the bottom Atlantic cannot be the result of an increasing input of fast sinking POC. The waters that feed the deep Atlantic in our model are formed between 55° and 80°N in the same basin (NADW) and between 70° and 47.5°S in the Southern Ocean [*Stocker et al.*, 1992b]. The new production in the NADW formation area drops to a minimum of 30% of its initial value when FI is maximum. Then it recovers to only 60% of this value at $t =$ 2 ka (solid line in Figure 5a). In the Southern Ocean, on the other hand, the new production is not significantly altered (long dashed line in Figure 5a). Therefore the PO_4 and $\delta^{13}C$ anomalies cannot be due to an increasing input of DOC_l in the source waters either.

The analysis above indicates that the PO_4 and $\delta^{13}C$ anomalies in Atlantic bottom waters result primarily from a decrease in the ventilation by newly formed NADW consistent with a reduction in $\Delta^{14}C$ [*Stocker and Wright*, 1996]. The reduced influence of NADW in the bottom Atlantic is accompanied by a stronger influence of waters of Antarctic origin [*Stocker et al.*, 1992b]. This would produce changes in bottom water PO_4 and $\delta^{13}C$ due to changes in the proportion of end-members with different preformed properties. This has no significant impact in our model, however, because the PO_4 and low $\delta^{13}C$ anomalies simulated in the bottom Atlantic can be entirely explained by the AOU change.

3.2.2. Changes in preformed PO_4 and $\delta^{13}C$ in the NADW formation area. The surface PO_4 in the northern North Atlantic first decreases to near zero at the time of maximum FI and then increases until the resumption of the thermohaline overturning (solid line in Figure 5c). These variations are due to an imbalance between the biological uptake and the deepwater supply of PO_4 when the freshwater cap is present in the North Atlantic (Figure 4e). When the FI is increasing, the supply of PO_4 is reduced, and the surface PO_4 is biologically consumed. Thereafter, when the FI is decreasing, the mixed layer deepens by convection (Figure 5b), bringing to the surface PO_4 which has accumulated at depth in the meantime (dashed line in Figure 5c) and increasing the amount of PO_4 that is recycled in this layer.

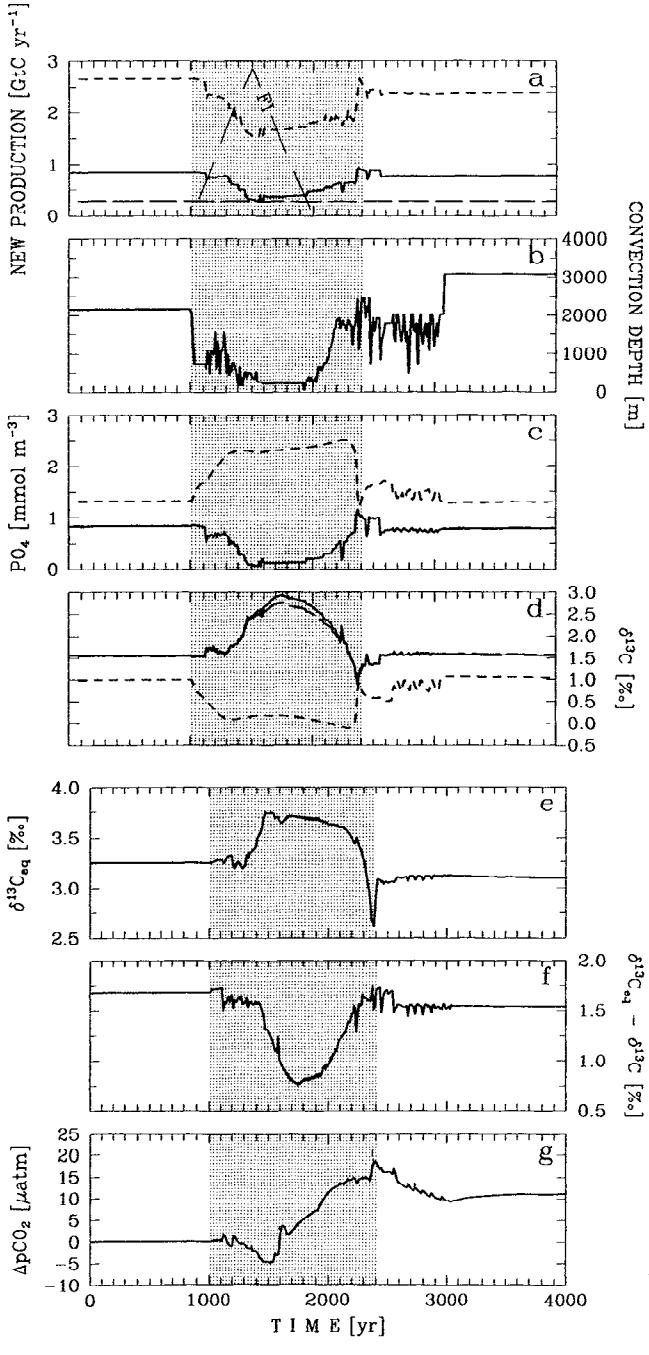

Figure 5. Timeseries in the reference simulation: (a) new production in the North Atlantic Deep Water (NADW) formation area between 55° and 80°N (solid line), Southern Ocean between 70° and 47.5°S (long-dashed line), and whole Atlantic between 70°S and 80°N (short-dashed line); (b) convection depth in the NADW formation area; (c) PO_4 in the NADW formation area at the surface (solid line) and 3750 m (short-dashed line); (d) $\delta^{13}C$ in the NADW formation area at the surface simulated with a variable α_{org} (solid line) and constant α_{org} (long-dashed line) and at 3750 m with a variable α_{org} (short-dashed line); (e–f) $\delta^{13}C_{eq}$ and isotopic disequilibrium in the NADW formation area; (g) anomaly of ocean mean surface pCO_2 (short-dashed line) and atmospheric pCO_2 (solid line). In Figure 5a, FI is the freshwater input with a range of 0–0.4 Sv. The shaded areas denote the period during which the Atlantic thermohaline circulation (THC) is altered.

The surface $\delta^{13}C$ in the northern North Atlantic first increases up to a maximum of 2.9‰ at $t = 1.75$ ka, i.e., approximately 200 years after the minimum in surface PO_4. Then it decreases until the resumption of the THC (solid line in Figure 5d). We describe the photosynthetic uptake of ^{13}C by a Rayleigh process with a fractionation factor α_{org} decreasing with decreasing ambient temperature [*Rau et al.*, 1989]. The large initial enrichment in surface $\delta^{13}C$ cannot result from a stronger photosynthetic uptake because new production in the NADW formation area drops during this period (Figure 5a). However, α_{org} decreases in this area because of a cooling of several degrees (Figure 4d), and this increasing isotopic selectivity could potentially contribute to the $\delta^{13}C$ enrichment. In order to identify this effect we conduct a simulation where α_{org} is fixed everywhere in the model to its initial steady state value. The difference between the surface $\delta^{13}C$ in the NADW formation area simulated with a variable and a constant α_{org} (long-dashed line in Figure 5d) reaches a maximum of only 0.2‰. Thus the enhanced photosynthetic fractionation due to cooling is insufficient to account for the $\delta^{13}C$ enrichment in dissolved inorganic carbon predicted in the northern North Atlantic (maximum of ~1.4‰).

In addition to photosynthesis the $\delta^{13}C$ of ocean surface DIC is further influenced by the air-sea gas exchange [*Broecker and Maier-Reimer*, 1992; *Lynch-Stieglitz et al.*, 1995]. To isolate this effect, we consider the $\delta^{13}C$ expected from a complete isotopic equilibrium with the atmosphere, $\delta^{13}C_{eq}$. Cooling during the first half of the FI induces a sharp increase of $\delta^{13}C_{eq}$ in the NADW formation area (Figure 5e). This increase, however, is lower than the simulated $\delta^{13}C$ enrichment, resulting in a drop of the isotopic disequilibrium, $\delta^{13}C - \delta^{13}C_{eq}$, from 1.7‰ at $t = 1$ ka to only 0.8‰ when $\delta^{13}C$ reaches its maximum (Figure 5f). This reduction is related to a increase in the ratio of air-sea gas exchange to ocean mixing rate in the NADW formation area when the THC collapses [*Broecker and Maier-Reimer*, 1992]. It permits better equilibration with the atmosphere although additional sea ice covers a maximum of 20% of this area at $t = 1.7$ ka (not shown). Thus the rise in preformed $\delta^{13}C$ in the northern North Atlantic stems mainly from a longer residence time of the waters at the surface. The subsequent drop, on the other hand, is associated with the deepening of the mixed layer which brings low-$\delta^{13}C$ waters to the surface ($\delta^{13}C$ has decreased at depth in the meantime; short-dashed line in Figure 5d) and lengthens the equilibration time with the atmosphere.

3.3. Changes in Atmospheric pCO_2

In the model the atmospheric partial pressure of CO_2, pCO_2^a, is exclusively determined by the equilibrium with the ocean mean surface pCO_2, $\langle pCO_2^w \rangle$, because the fluxes of total CO_2 between the atmosphere and the land biosphere are constant and the air-sea gas exchange coefficient is uniform (in the following, the angle brackets "<>" denote the ocean mean surface value of any property). Except during some episodes of very fast $\langle pCO_2^w \rangle$ changes, differences between pCO_2^a and $\langle pCO_2^w \rangle$ are insignificant (compare solid with dashed line in Figure 5g). This implies that the ocean and the atmosphere remain in chemical equilibrium during the transient experiments. Three major changes in pCO_2^a can be distinguished. First, pCO_2^a decreases slightly by 5 μatm from the start of the FI until the maximum discharge. This period is contemporaneous with the phase of the slowdown of the thermohaline circulation in the Atlantic (e.g. Figure 3b). Then pCO_2^a increases by about 25 μatm until approximately 400 years after the end of the FI when the THC suddenly and vigorously resumes. Finally, pCO_2^a decreases again to a new equilibrium value which is about 10 μatm higher than the initial steady state pCO_2^a. The initial and final pCO_2^a are different because the injection of freshwater has led to a new equilibrium distribution of physical (T and S) and chemical properties (DIC and ALK) in the surface waters.

We now examine the factors responsible for the changes in $\langle pCO_2^w \rangle$. Although some of these changes are relatively small (e.g., 5 μatm) and may hardly be detected in the paleoclimatic record, we will show that they arise from the compensation between much larger changes imparted by distinct oceanic processes at different geographic locations. The change in the partial pressure of CO_2 in each surface cell in the model is expressed as a linear combination of the changes in sea surface temperature, salinity, concentration of dissolved inorganic carbon, and alkalinity [*Takahashi et al.*, 1993]. With $\mathcal{T} \in \{T, S, \mathrm{DIC}, \mathrm{ALK}\}$; this change is computed as

$$\Delta pCO_{2,l}^{w} = \sum_{\mathcal{T}} \Delta pCO_2^{(\mathcal{T})} = \sum_{\mathcal{T}} \frac{\partial pCO_2}{\partial \mathcal{T}} \Delta \mathcal{T} \quad (3)$$

where DIC and ALK in the latter equation are the actual concentrations (i.e. they are not normalized to salinity), $\partial pCO_2/\partial T > 0$, $\partial pCO_2/\partial S > 0$, $\partial pCO_2/\partial \mathrm{DIC} > 0$, and $\partial pCO_2/\partial \mathrm{ALK} < 0$. We first test (3) with constant partial derivatives inferred from equations (2)–(5) of *Takahashi et al.* [1993] representative of ocean mean surface conditions. In this case the difference between $\langle \Delta pCO_{2,l}^w \rangle$ and $\langle \Delta pCO_2^w \rangle$ (with pCO_2^w computed from thermodynamical relationships of the seawater CO_2 system [*Marchal et al.*, 1998]) reaches a maximum of ~4 μatm. Because we have to interpret relatively small net fluctuations in $\langle pCO_2^w \rangle$, we adopt a second, more accurate approach where $\Delta pCO_{2,l}^w$ is calculated with time varying partial derivatives (see appendix). This approach provides a first-order estimate of the quantitative effects of T, S, DIC, and ALK changes on pCO_2^w. The difference between $\langle \Delta pCO_{2,l}^w \rangle$ and

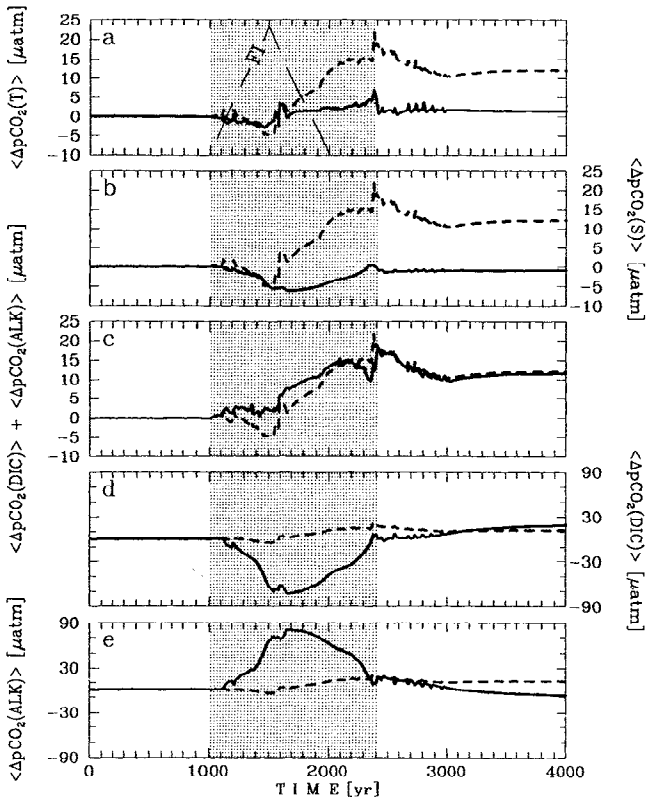

Figure 6. Ocean mean (a) $< \Delta pCO_2^{(T)} >$, (b) $< \Delta pCO_2^{(S)} >$, (c) $< \Delta pCO_2^{(DIC)} > + < \Delta pCO_2^{(ALK)} >$, (d) $< \Delta pCO_2^{(DIC)} >$, and (e) $< \Delta pCO_2^{(ALK)} >$ in the reference simulation (solid lines). The ocean mean surface $< \Delta pCO_{2,l}^{w} >$ is also shown in Figures 6a–6e (dashed-lines). Note the different scales for Figures 6a–6c and 6d–6e. In Figure 6a, FI is the freshwater input with a range of 0–0.4 Sv. The shaded areas denote the period during which the Atlantic THC is altered.

$\langle \Delta pCO_2^{w} \rangle$ reaches a maximum of only 1 μatm in this case, indicating that (3) is a fair approximation to the fully nonlinear dependence of pCO_2^{w}. In the following we use the latter approach to identify the causes of the $\langle pCO_2^{w} \rangle$ changes during the abrupt thermohaline oscillation.

The ocean mean changes $\left\langle \Delta pCO_2^{(T)} \right\rangle$ and $\left\langle \Delta pCO_2^{(S)} \right\rangle$ are 1 order of magnitude smaller than $\left\langle \Delta pCO_2^{(DIC)} \right\rangle$ and $\left\langle \Delta pCO_2^{(ALK)} \right\rangle$ (solid lines in Figure 6). The sum $\left\langle \Delta pCO_2^{(DIC)} \right\rangle + \left\langle \Delta pCO_2^{(ALK)} \right\rangle$ (Figure 6c) is, however, only about 3 times larger than the individual effects of temperature and salinity because $\frac{\partial pCO_2}{\partial DIC} \Delta DIC \approx -\frac{\partial pCO_2}{\partial ALK} \Delta ALK$ [*Takahashi et al.*, 1993]. This implies that the variations of each of the four factors (T, S, DIC and ALK) must be taken into account when interpreting the changes in the ocean mean surface pCO_2. Consider, for example, the relatively large $\langle pCO_2^{w} \rangle$ increase of 26 μatm from the maximum of freshwater input (t = 1.5 ka) until the resumption of the THC in the Atlantic (t = 2.4 ka). This increase is associated with an increase in the ocean mean sea surface temperature (8 μatm), salinity (6 μatm), and DIC concentration (74 μatm). These three effects are counteracted by an increase in $\langle$ALK$\rangle$ during the same period (−61 μatm) (Table 2).

3.3.1. Effect of temperature changes. A first major consequence of the collapse of the thermohaline circulation in the model is a strong cooling in the northern North Atlantic (Figure 4d). Cooling in the region north of 20°N in the Atlantic creates a strong sink with $\Delta pCO_2^{(T)}$ reaching a minimum of $\frac{\partial pCO_2}{\partial T} \Delta T \approx$ −35 μatm. The impact of this sink on the atmospheric pCO_2 is muted, however, because this region occupies

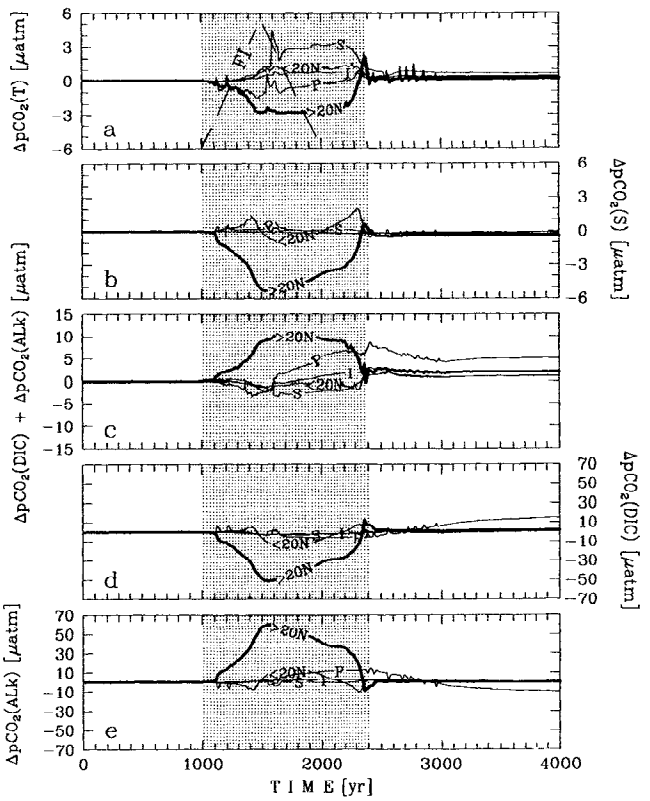

Figure 7. (a) $\Delta pCO_2^{(T)}$, (b) $\Delta pCO_2^{(S)}$, (c) $\Delta pCO_2^{(DIC)}$ + $\Delta pCO_2^{(ALK)}$, (d) $\Delta pCO_2^{(DIC)}$, and (e) $\Delta pCO_2^{(ALK)}$ in different areas in the reference simulation: the Atlantic between 47.5°S and 20°N (<20N) and between 20° and 80°N (>20N), the Southern Ocean between 70° and 47.5°S (S), the Indian Ocean between 47.5°S and 20°N (I), and the Pacific Ocean between 47.5°S and 55°N (P). Values are weighted according to surface area in order to highlight their actual contribution to the anomaly of atmospheric pCO_2. Note the different scales in Figures 7a–7b, 7c, and 7d–7e. In Figure 7a, FI is the freshwater input with a range of 0–0.4 Sv. The shaded areas denote the period during which the Atlantic THC is altered.

Table 2. Ocean Mean pCO_2 Anomalies Due to Changes in Sea Surface T, S, DIC, and ALK in the Reference Perturbation

Time Interval	$\langle \Delta pCO_2^{(T)} \rangle$	$\langle \Delta pCO_2^{(S)} \rangle$	$\langle \Delta pCO_2^{(DIC)} \rangle$ [a]	$\langle \Delta pCO_2^{(ALK)} \rangle$ [a]	$\langle \Delta pCO_2^{w} \rangle$
From 1.0 to 1.5 ka	-1	-5	-67 (0.07)	69 (0.18)	-5
From 1.5 to 2.4 ka	8	6	74 (0.04)	-61 (-0.12)	26
From 2.4 to 3.0 ka	-5	-1	0 (-1.92)	-5 (-7.36)	-12
From 1.0 to 3.0 ka	2	-1	7 (-1.00)	3 (0.14)	9

Anomalies are in μatm.

[a]Values in brackets are ratios of the change in the ocean mean surface salinity-normalized DIC (ALK) to the change in the ocean mean surface DIC (ALK) for the different time intervals. A low absolute value indicates that a relatively large fraction of the change in the ocean mean surface DIC (ALK), and hence of $<\Delta pCO_2^{(DIC)}>$ ($<\Delta pCO_2^{(ALK)}>$), is correlated to the change in surface salinity. The other values are obtained from the linear approximation (3) in the text.

only ~10% of the total ocean area and the impact is offset by a warming elsewhere, mostly in the Southern Ocean (Figure 7a). When the THC resumes (at $t \approx 2.3$ ka), $\Delta pCO_2^{(T)}$ north of 20°N in the Atlantic sharply increases. This is due to the enhanced northward heat transport and to mixing with deep waters which are relatively warm in this region when the Atlantic THC is collapsed (Figure 4d).

The warming of surface waters in the Southern Ocean occurs when the thermohaline overturning in the Atlantic is suppressed and is interrupted when this overturning resumes (compare, for example, Figure 3b with Figure 7a). The warming is due, at least partly, to an increasing supply of heat from the thermal inversion which is present in the top 500 m in the initial steady state of the model (solid line in Figure 8a). In the initial steady state this thermal inversion is stabilized by a strong vertical gradient in salinity (solid line in Figure 8b). When the Atlantic thermohaline overturning declines, the temperature increases, and the salinity decreases at depth in the Southern Ocean (short-dashed lines in Figures 8a–8b). This alters the static stability of the water column and leads to a large convective event at $t \approx 1.6$ ka (dash–dotted lines in Figures 8a–8b). During this event the thermal inversion is completely eroded, a large amount of heat is suddenly released to the atmosphere, and the atmospheric pCO_2 rises almost instantaneously by ~7 μatm (Figure 5g).

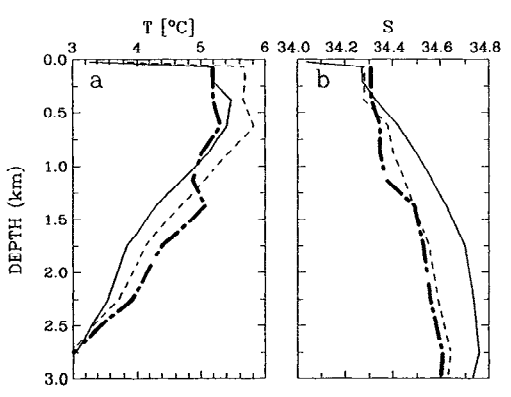

Figure 8. Average vertical profiles of (a) temperature and (b) salinity in the Southern Ocean for the reference simulation at $t = 1$ ka (solid line; start of FI), 1.5 ka (dashed line; peak of FI) and 1.6 ka (long-dashed, short-dashed line). The thermal inversion in the upper water column is completely eroded between $t = 1.5$ and 1.6 ka.

3.3.2. Effect of salinity, DIC, and ALK changes. A second major consequence of the collapse of the thermohaline circulation is a pronounced freshening in the North Atlantic (Figure 4e). This freshening is induced by the direct effect of the FI, but negative $E - P - R$ values in this region amplify the salinity anomaly when the THC weakens (see the positive feedback identified by [*Bryan*, 1986]). Thus $\Delta pCO_2^{(S)}$ varies primarily in the North Atlantic (Figure 7b). In the region north of 20°N in the Atlantic, $\Delta pCO_2^{(S)}$ decreases until the maximum FI and then increases when the freshwater cap is progressively eroded. When the thermohaline overturning resumes (at $t \approx 2.3$ ka), it rises abruptly because of the enhanced northward transport of salt and to mixing with deep waters which are relatively saline in this region (Figure 4e).

$\Delta pCO_2^{(DIC)}$ and $\Delta pCO_2^{(ALK)}$ reflect changes in the prescribed freshwater input, ocean biological cycling and transport. $\Delta pCO_2^{(DIC)}$ further reflect changes in the air-sea flux of CO_2. As for $\Delta pCO_2^{(S)}$, $\Delta pCO_2^{(DIC)}$, and $\Delta pCO_2^{(ALK)}$ vary predominantly in the North Atlantic (Figures 7d–7e). In the region north of 20°N in this basin, $\Delta pCO_2^{(DIC)}$ decreases and $\Delta pCO_2^{(ALK)}$ increases from the start of the FI until the maximum discharge; then, $\Delta pCO_2^{(DIC)}$ increases and $\Delta pCO_2^{(ALK)}$ decreases until the resumption of the thermohaline overturning. In this region at the surface the changes in DIC and ALK, which are very pronounced, are much larger than

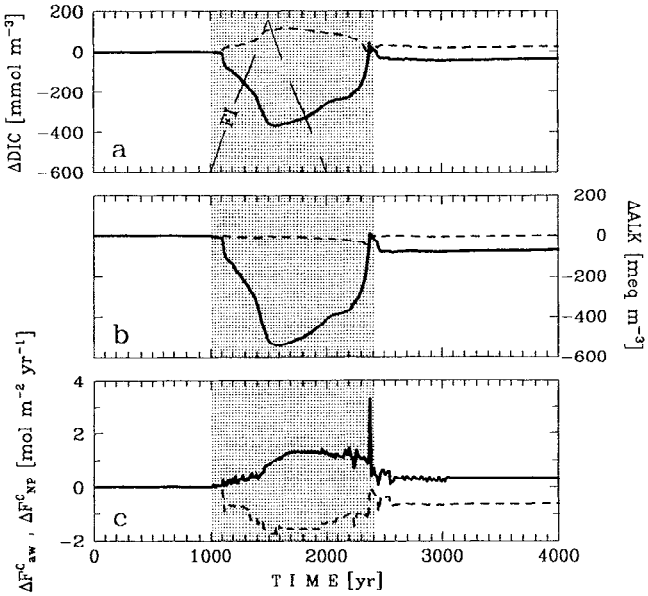

Figure 9. Timeseries of different anomalies north of 20°N in the Atlantic in the reference simulation: (a) surface DIC, (b) surface ALK and (c) air-to-sea CO_2 flux (solid line). The surface DIC and ALK normalized to salinity are shown in Figures 9a and 9b, respectively, and new production is shown in Figure 9c (dashed line). In Figure 9a, FI is the freshwater input with a range of 0–0.4 Sv. The shaded areas denote the period during which the Atlantic THC is altered.

the changes in salinity-normalized DIC and ALK (compare solid with dashed lines in Figures 9a–9b). This indicates that most of $\Delta pCO_2^{(DIC)}$ and $\Delta pCO_2^{(ALK)}$ are correlated to salinity changes (see also Table 2). On the other hand, the mixed layer north of 20°N in the Atlantic takes up an increasing amount of atmospheric CO_2 when the THC declines (solid line in Figure 9c). This is illustrated by a rise in salinity-normalized DIC (Figure 9a) and compensates to some extent the effect of freshwater dilution on DIC. The subsequent decrease in the salinity-normalized DIC results, at least partly, from the increase in new production (dashed line in Figure 9c).

4. Sensitivity Analyses

4.1. Ocean Circulation Change

4.1.1. PO_4 and $\delta^{13}C$ in the bottom Atlantic. We now consider timeseries of PO_4 and $\delta^{13}C$ in the deepest and northernmost grid cell in the Atlantic simulated for FI with different values of V and D and applied at various latitudes (Figures 10a–10b). This cell is selected because it is directly under the influence of NADW. PO_4 and $\delta^{13}C$ anomalies simulated at the same depth more to the south in the North Atlantic are qualitatively similar and therefore do not alter the observations below. PO_4 always increases and $\delta^{13}C$ always decreases in the bottom water when the thermohaline overturning is reduced. There is, however, no simple relationship between the amplitude of the PO_4 and $\delta^{13}C$ anomalies and the amplitude of the reduction in the Atlantic overturning rate (Ψ_{max}). For instance, PO_4 and $\delta^{13}C$ anomalies reach similar maxima when Ψ_{max} is reduced by 90% (reference perturbation) or 45%–50% (when $V = 4 \times 10^6$ km^3 or when $D = 1.5$ kyr). These anomalies also reach similar maxima when the same FI is applied in the North Atlantic or along the Antarctic perimeter in which case Ψ_{max} is depressed by only 35% (Figures 10a–10b). The lack of a linear relationship between the bottom water anomalies and THC reduction is due to the fact that PO_4 enrichment and $\delta^{13}C$ depletion in these waters occur as soon as ventilation by PO_4-poor and $\delta^{13}C$-rich NADW no longer balances the oxidation of organic matter at depth. This ventilation stops very abruptly because of the abrupt cessation of the convective activity in the northern North Atlantic (threshold effect; see Figure 5b).

The simulations with a reduced but still significant production of NADW exhibit a shallower thermohaline

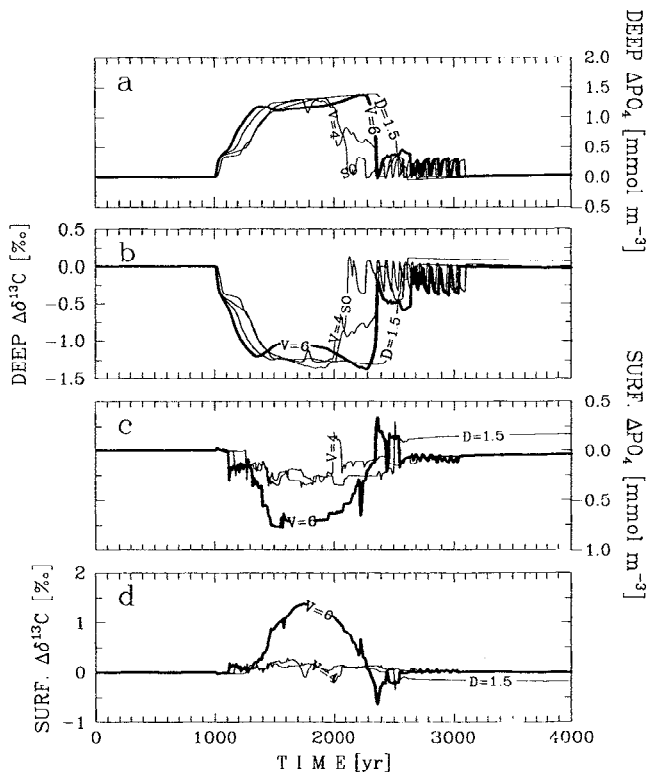

Figure 10. Timeseries of the anomaly of (a) PO_4 and (b) $\delta^{13}C$ at 3750 m and 72.5°N in the Atlantic and of (c) PO_4 and (d) $\delta^{13}C$ at the surface in the NADW formation area (55°–80°N). The different curves correspond to the reference simulation (thick line) and to three other simulations where $V = 4 \times 10^6$ km^3, $D =$ 1.5 kyr, or where the FI applied in the Southern Ocean (70°–62.5°S).

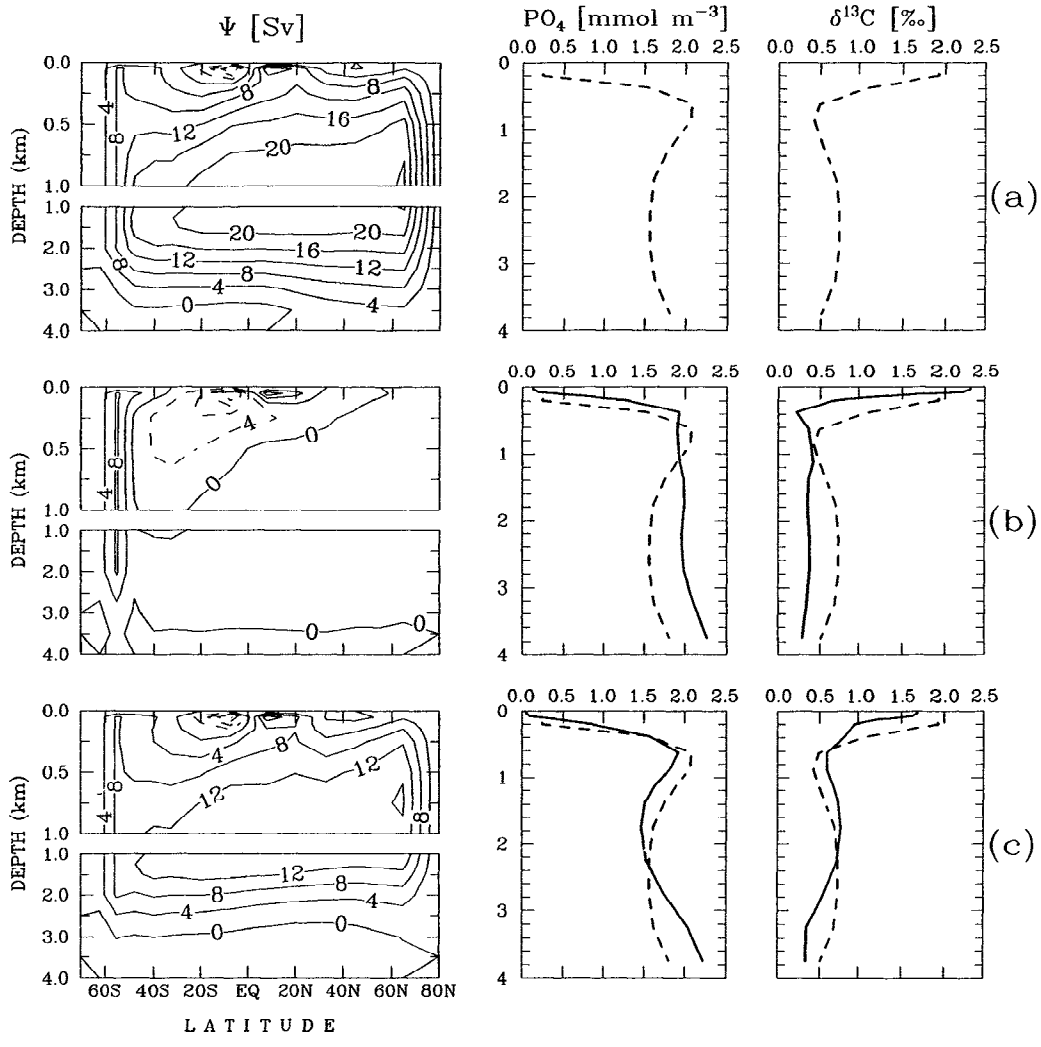

Figure 11. Latitude-depth distributions of the stream function and vertical profiles of PO_4 and $\delta^{13}C$ at 38.75°N in the Atlantic: (a) initial steady state, (b) reference simulation with $V = 6 \times 10^6$ km^3, $D = 1$ kyr, and FI applied in the Atlantic between 32.5° and 45°N (at $t = 2$ ka), and (c) simulation with $D = 2.5$ kyr and the other FI characteristics of the reference simulation (at $t = 2.3$ ka). In Figures 11b–11c, the dashed vertical profiles correspond to the initial steady state.

overturning compared to the initial steady state (Figure 11). In this case the PO_4 enrichment and $\delta^{13}C$ depletion at midlatitudes in the bottom Atlantic are accompanied by PO_4 depletion and $\delta^{13}C$ enrichment in the intermediate waters. This results in an increasing vertical gradient of these properties below 1 km in the water column (Figure 11c). Thus, although similar anomalies of PO_4 and $\delta^{13}C$ are simulated in the bottom North Atlantic with quite distinct drops in the THC intensity, negative PO_4 and positive $\delta^{13}C$ anomalies occur at intermediate levels when the Atlantic overturning is only partly reduced and occurs at shallower depths.

4.1.2. Preformed PO_4 and $\delta^{13}C$ in the NADW formation area. Timeseries of surface PO_4 and $\delta^{13}C$ in the northern North Atlantic simulated for FI with different V, D, and latitudes are given in Figures 10c–10d. In these simulations the preformed PO_4 always decreases and then increases. The preformed $\delta^{13}C$, however, does not systematically exhibit a concomitant enrichment and subsequent depletion as for example in the reference simulation. This further demonstrates that the anomalies of surface PO_4 and $\delta^{13}C$ in the northern North Atlantic are determined by different processes.

4.1.3. Atmospheric pCO_2. Simulations for FI with different V, D, and latitudes all exhibit an increase of pCO_2^a when the Atlantic THC is modified (Figure 12). As a general rule, this increase is higher for a larger volume of freshwater discharged and for a shorter duration of the FI. It is preceded by a pCO_2^a decrease of smaller amplitude if the freshening is sufficiently large. This

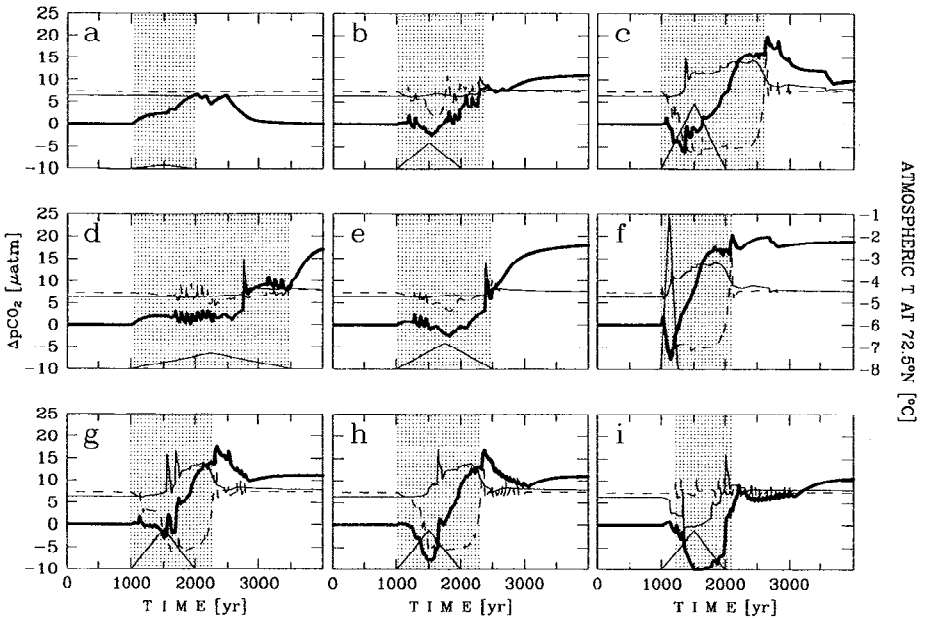

Figure 12. Timeseries of the anomaly of atmospheric pCO_2 (thick solid line), atmospheric temperature at 72.5°N (short-dashed line) and mean sea surface temperature in the Southern Ocean (thin solid line). The different panels correspond to (a) $V = 0.5 \times 10^6$ km^3; (b) 4×10^6 km^3; (c) 10×10^6 km^3; (d) $D = 2.5$ kyr; (e) 1.5 kyr; (f) 0.25 kyr; (g) FI in the Atlantic between 45° and 55°N; (h) 20°–32.5°N; and (i) along the Antarctic perimeter. The other FI characteristics are those of the reference perturbation ($V = 6 \times 10^6$ km^3, $D = 1$ kyr and FI applied in the Atlantic between 32.5°–45°N). The mean sea surface temperature in the Southern Ocean is reported with a range of 0°–7°C. The shaded area denotes the period during which the Atlantic THC is altered in each simulation.

results in an asymmetric V-shaped evolution of pCO_2^a as apparent, for example, in the reference perturbation (Figure 5g). This evolution is also predicted when the FI is applied along the Antarctic perimeter (Figure 12i). In this case, however, the initial pCO_2^a decrease is larger and the subsequent pCO_2^a increase is lower than if the same FI is prescribed in the North Atlantic.

In the reference perturbation a significant contributor to the pCO_2 anomaly is a warming of the surface waters in the Southern Ocean. Simulations for FI with different V, D, and latitudes in the North Atlantic suggest that this is a robust feature in our model (thin solid line in Figure 12c, 12f, and 12g–12h). The prediction of an opposite temperature evolution between the North Atlantic and the Southern Ocean is consistent with the "NADW-Antarctic" connection hypothesized by *Crowley* [1992] on the basis of observations and previous modeling studies.

4.2. Changes in Biological Cycling

The global new production decreases by ~20% in the reference perturbation (solid line in Figure 13a) mainly because of a reduction in the Atlantic (Figure 5a). There, the delivery of PO_4 from deep waters to the euphotic zone is drastically reduced by the enhanced stability of the water column due to freshwater capping (Figures 5b–5c).

In order to assess the sensitivity of the model responses to the changes in biological cycling we conduct an additional simulation where the rates of production and oxidation of organic matter and the rates of production and dissolution of $CaCO_3$ are kept fixed at their initial steady state values. This simulation may produce negative PO_4 because the nutrient is biologically consumed at a constant rate in the euphotic zone. It is, nevertheless, instructive because it provides insight into the effect of changes in the biological fluxes on the anomalies of oceanic PO_4 and $\delta^{13}C$ and of atmospheric pCO_2 which are predicted when the thermohaline overturning is altered. When biological cycling is kept constant, the biogeochemical responses to the THC change are drastically amplified (dashed lines in Figures 13b–13d). Specifically, the $\delta^{13}C$ surface enrichment and bottom depletion in the North Atlantic are much larger. Also, the V-shaped evolution of the atmospheric pCO_2, with a minimum now occurring at the time of THC resumption, is much more pronounced compared to the reference perturbation. The new production therefore exerts an important negative feedback in our transient experiments. Its decrease reduces the uptake and re-

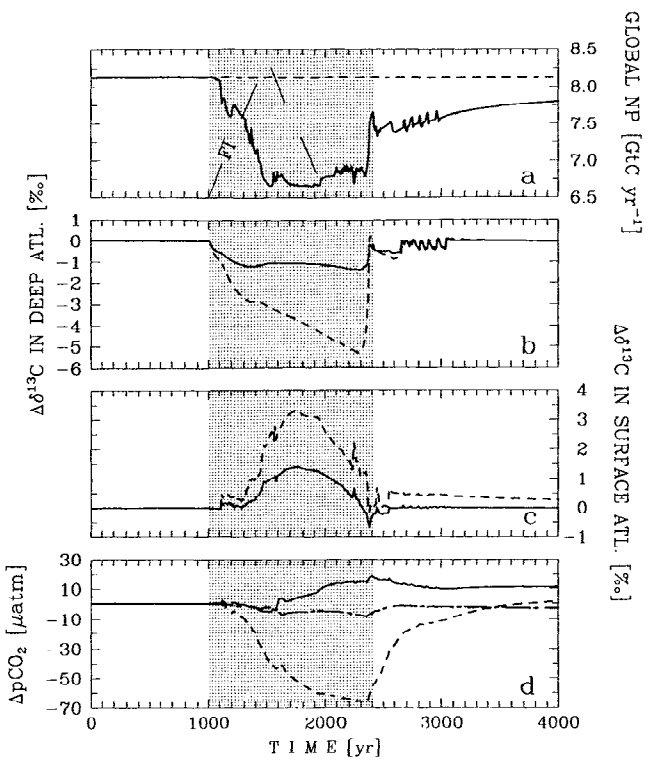

Figure 13. Timeseries of (a) global new production, (b) $\delta^{13}C$ anomaly at 3750 m and 72.5°N in the Atlantic, (c) $\delta^{13}C$ anomaly at the surface in the NADW formation (55°-80°N), and (d) anomaly of atmospheric pCO_2. The different curves correspond to the reference simulation (solid line), the simulation with constant biological cycling (dashed line), and the simulation without biological cycling (long-dashed, short-dashed line; only in Figure 13d). In Figure 13a, FI is the freshwater input with a range of 0–0.4 Sv. The shaded areas denote the period during which the Atlantic THC is altered.

lease of isotopically light carbon at the surface and at depth, respectively, thereby counteracting the surface $\delta^{13}C$ enrichment and deep $\delta^{13}C$ depletion in the North Atlantic. In addition, the decrease in new production damps the variations in surface DIC brought about by the FI thereby reducing the amplitude of pCO_2^a changes.

We consider a final simulation where the ocean is now abiotic. An initial steady state of the model is produced keeping all biological fluxes equal to zero in the five-step procedure described in section 2.3. In this simulation the changes in atmospheric pCO_2 are qualitatively similar to that with constant biological fluxes but are very small (dash-dotted line in Figure 13d). This is due to a different evolution of $\left\langle \Delta pCO_2^{(DIC)} \right\rangle + \left\langle \Delta pCO_2^{(ALK)} \right\rangle$ which exhibits a decrease, instead of an increase in the reference simulation, between the FI maximum and the time of THC resumption (not shown). This is another illustration that ocean biological cycling would have a major impact on pCO_2^a during THC changes.

5. Discussion and Conclusions

We have used a simplified circulation-biogeochemical model to investigate the impact of fast changes in the ocean thermohaline circulation on the distribution of PO_4 and $\delta^{13}C$ in the major oceanic basins and on the concentration of CO_2 in the atmosphere. Several processes that are potentially important for the kind of climate events explored here are crudely described or even omitted. This allowed us to obtain a dynamical model that can be integrated for several thousand years and to perform systematic sensitivity studies. Deficiencies of the ocean and atmosphere models have already been discussed [e.g., *Wright and Stocker*, 1993]. In addition, our description of the ocean carbon cycle is also highly simplified as explained by *Marchal et al.* [1998]. As an example, there is no preservation of $CaCO_3$ in deep-sea sediments and the effect of the production of respiratory CO_2 on $CaCO_3$ dissolution in those sediments [*Emerson and Bender*, 1981] is thus not taken into account. This places limitations on the present model because deep-sea records document significant variations in the depth of the sedimentary lysocline in conjunction with marine isotope stages during the late Pleistocene [e.g., *Farrell and Prell*, 1989]. This effect has most likely contributed to the glacial-to-interglacial increases in atmospheric pCO_2 [*Broecker and Peng*, 1987; *Archer and Maier-Reimer*, 1994]. The timescale investigated here is of the order of ~1 kyr, which is comparable to the e-folding time of ~2.5 kyr for $CaCO_3$ compensation [*Broecker and Peng*, 1987] but shorter than the timescale of the transition from full glacial-to-interglacial conditions (between ~7–10 kyr). It is much shorter, on the other hand, than the oceanic residence time of phosphorus estimated to ~100 kyr [*Froelich et al.*, 1982] which justifies the assumption of a constant ocean inventory of PO_4 in the model (note that it is implicitly assumed that the ocean inventory of nitrate is constant as well).

In spite of these limitations our model simulations have implications for the interpretation of the abrupt variability documented in deep-sea sediment and polar ice records for the last glacial period. These possible implications are discussed below.

5.1. Deep-Sea Records of Benthic Foraminiferal Cd/Ca and $\delta^{13}C$

The model exhibits three prominent responses to the addition of freshwater at the surface in the North Atlantic. First, PO_4 rises and $\delta^{13}C$ becomes lighter in the bottom waters in this basin. This is consistent with the drop in benthic foraminiferal $\delta^{13}C$ documented during Heinrich events in North Atlantic cores [*Keigwin and Lehman*, 1994; *Vidal et al.*, 1997; *Zahn et al.*, 1997]. For the Younger Dryas cold phase (YD), which may also have been triggered by glacial FI [e.g., *Broecker*

et al., 1990], several studies reported a Cd/Ca increase and $\delta^{13}C$ decrease in the bottom North Atlantic [*Boyle and Keigwin*, 1987; *Keigwin et al.*, 1991; *Keigwin and Lehman*, 1994]. Other authors, however, did not find a decrease in benthic foraminiferal $\delta^{13}C$ in other cores raised from the North Atlantic thereby challenging the view that NADW production was low during the YD [*Jansen and Veum*, 1990; *Veum et al.*, 1992; *Sarnthein et al.*, 1994]. In our model the PO_4 enrichment and $\delta^{13}C$ depletion are clearly related to a drastic reduction in the ventilation of the bottom Atlantic by newly formed NADW. Although this supports the conventional interpretation of deep-sea records of benthic foraminiferal Cd/Ca and $\delta^{13}C$, PO_4 increases and $\delta^{13}C$ decreases of comparable amplitude are also simulated when the thermohaline overturning is much less reduced. This model prediction is due to a threshold beyond which the ventilation by PO_4-poor and $\delta^{13}C$-rich NADW becomes insufficient to compensate the PO_4 enrichment and $\delta^{13}C$ depletion at depth because of the oxidation of organic matter. This would imply that similar changes in benthic foraminiferal Cd/Ca or $\delta^{13}C$ along a sedimentary column do not necessarily reflect similar changes in the formation rate of NADW. Alternatively, distinct changes in benthic foraminiferal Cd/Ca or $\delta^{13}C$ do not necessarily reflect proportional changes in the formation rate of end-members.

Second, concomitant with a PO_4 enrichment and $\delta^{13}C$ depletion in the bottom waters, PO_4 decreases and $\delta^{13}C$ increases between ~0.5–2.5 km in the midlatitude Atlantic when the thermohaline overturning is only partly reduced and occurs at shallower depths. The resulting increasing vertical gradients of PO_4 and $\delta^{13}C$ are reminiscent of chemical and isotopic reconstructions for the last glacial maximum (LGM) [*Boyle*, 1988; *Curry et al.*, 1988]. Although our effort is not to simulate the climate conditions at the LGM, it does support the contention that compared to present-day conditions, the LGM was characterized by a smaller and shallower production of deep waters in the northern North Atlantic [*Boyle*, 1988; *Curry et al.*, 1988].

Third, both the surface PO_4 and $\delta^{13}C$ in the NADW formation area change substantially when the thermohaline circulation in the Atlantic collapses. PO_4 first decreases owing to an imbalance between the biological uptake and the supply of PO_4 from deep waters. The isotopic ratio $\delta^{13}C$, on the other hand, first increases because of a longer residence time of the surface waters in the northern North Atlantic. Mixing with deep waters and a smaller residence time when the THC resumes eventually reestablish the initial PO_4 and $\delta^{13}C$. These PO_4 and $\delta^{13}C$ anomalies (>0.5 mmol m^{-3} and >1‰ in the reference perturbation) are significant compared to the difference observed today between the surface PO_4 and $\delta^{13}C$ in the Southern Ocean and in the northern North Atlantic [*Conkright et al.*, 1994; *Kroopnick*, 1985]. Thus these anomalies also may have profound implications for the interpretation of deep-sea records of benthic foraminiferal Cd/Ca and $\delta^{13}C$, where it is commonly assumed that the changes in preformed PO_4 and $\delta^{13}C$ are minor compared to changes brought about by mixing near the bottom between water masses of different chemical and isotopic signature. For instance, the abrupt PO_4 decrease and $\delta^{13}C$ increase in the bottom Atlantic simulated when the THC resumes (dashed lines in Figures 5c–5d) are clearly associated with the reinjection at depth of the surface waters which have been previously depleted in PO_4 and enriched in $\delta^{13}C$. This effect is similar to the "store and advect" scenario proposed by *Lehman et al.* [1993] to explain abrupt changes in records of benthic foraminiferal $\delta^{18}O$. Thus the present results support the contention that the air-sea exchange, for instance, may represent a significant source of variability in deep sea records of foraminiferal $\delta^{13}C$ [*Charles et al.*, 1993].

5.2. Polar Ice Records of CO_2

The model simulations presented here allowed us to analyze further the hypothesis that ocean circulation changes can impart significant abrupt variations in the atmospheric pCO_2 [*Siegenthaler and Wenk*, 1984, herein referred to as SW84]. The net effect of a reduction in the THC would be a pCO_2^a increase instead of the pCO_2^a decrease predicted by SW84 on the basis of a four-box model. In this latter model the impact of changes in sea surface temperature and salinity on pCO_2^a and the possible impact of THC change on new production in high-latitude waters are not included. Here the increase in the ocean mean sea surface T and S are responsible for ~ 50% of the pCO_2^a increase from $t = 1.5$ to 2.4 ka (Table 2). Moreover, freshwater capping in the North Atlantic reduces the nutrient recharge from the deep and leads to surface PO_4 levels well below that which would be required to saturate natural phytoplankton communities (i.e., $PO_4 < K_{PO_4}$, indicating that PO_4 may become limiting in this region). Interestingly, the experiment with constant biological cycling predicts a pCO_2^a decrease when the THC is reduced, consistent with SW84. This leads us to conclude that in addition to a difference in model structure and assumptions, the discrepancy between our prediction and that of SW84 is due to a different treatment of the new production in these waters.

The present results also help us to interpret short-term variations in the atmospheric pCO_2 as reconstructed on the basis of high-resolution CO_2 measurements in air entrapped in the Byrd ice core (West Antarctica). First, using CH_4 as a stratigraphic marker, *Blunier et al.* [1997] synchronized the Byrd pCO_2 record and the $\delta^{18}O$ record from Greenland Ice Core Project (GRIP; central Greenland) for the period cor-

responding to the last deglaciation. This indicated that the atmospheric pCO_2 has increased during the entire Younger Dryas (characterized by $\delta^{18}O$ minima in the Greenland record). Our simulations are qualitatively consistent with this observation and indicate as well a pCO_2^a increase during the cold period in the northern North Atlantic.

Second, from a stratigraphic correlation of the Byrd record with deep-sea sediment and GRIP records, *Stauffer et al.* [1998] reported that pCO_2^a increased by ~20 μatm within 2 kyr after Heinrich events 4–5. Our simulations are also qualitatively consistent with these observations if one considers that pCO_2^a in our model starts to increase from the coldest period in the northern North Atlantic (Figure 12) and that the Heinrich events are concomitant with the culmination of $\delta^{18}O$ minima and followed by a $\delta^{18}O$ increase in the Greenland record [*Bond et al.*, 1993]. A quantitative comparison between ice core CO_2 data and the predicted atmospheric pCO_2 is delicate, however, because of the poor observational constraints on the state of the thermohaline circulation just before the YD and Heinrich events.

On the basis of a simple Michaelis-Menten description for new production our results imply that the marine productivity, if mostly determined by the nutrient content of surface waters, should be a necessary ingredient in models intended to simulate pCO_2^a changes during abrupt climate transitions.

Appendix A: Description of Model Components

A1. Atmosphere

Given the timescales investigated here ($\gg$1 year), the atmosphere is considered as a well-mixed reservoir. The partial pressure pCO_2^a (in μatm) is hence related to the total atmospheric inventory of $CO_2 \equiv {}^{12}CO_2 + {}^{13}CO_2$ (I_a^C, in mol C) by $pCO_2^a = I_a^C P_a m_a/(4\pi a^2 H_a \rho_a)$, where $P_a = 10^6$ μatm is the atmospheric pressure, m_a = 28.964 gr mol^{-1} is the molecular weight of air, a is Earth's radius, H_a = 8320 m is a scale height of the atmosphere and $\rho_a = 1.225 \times 10^3$ gr m^{-3} is the air density. Likewise, the concentration of ${}^{13}CO_2$ in the atmosphere, ${}^{13}CO_2^a$ (in mol m^{-3}), is related to the total atmospheric inventory of ${}^{13}CO_2$ (I_a^{13C}, in mol C) by ${}^{13}CO_2^a = I_a^{13C}/(4\pi a^2 H_a)$. The atmospheric $\delta^{13}C$ is computed from the two former equations.

The mass balances for I_a^C and I_a^{13C} are written as

$$\frac{dI_a^C}{dt} = \int_A (F_{wa}^C - F_{aw}^C)\, dA + \phi_{ba}^C \quad \text{(A1)}$$

$$\frac{dI_a^{13C}}{dt} = \int_A (R_w \alpha_{wa} F_{wa}^C - R_a \alpha_{aw} F_{aw}^C)\, dA + \phi_{ba}^{13C} \quad \text{(A2)}$$

where F_{wa}^C and F_{aw}^C are the gross fluxes of CO_2 from sea-to-air and from air-to-sea, R_w and R_a are the ${}^{13}C/({}^{12}C+{}^{13}C)$ ratio of ocean surface DIC and atmospheric CO_2, α_{wa} and α_{aw} are fractionations factors for the sea-to-air and air-to-sea gas transfer, ϕ_{ba}^C and ϕ_{ba}^{13C} are the net fluxes of CO_2 and ${}^{13}CO_2$ from the land biosphere to the atmosphere, and A is the total ocean surface. The calculation of the air-sea fluxes of CO_2 and ${}^{13}CO_2$ are described by *Marchal et al.* [1998]. We detail below how the biospheric fluxes ϕ_{ba}^C and ϕ_{ba}^{13C} are obtained.

A2. Land Biosphere

The land biosphere component adopted here is that of *Siegenthaler and Oeschger* [1987]. This component consists of four carbon pools of different sizes and turnover times: ground vegetation plus leaves, wood, detritus, and soils. The inventories and fluxes of total C $\equiv {}^{12}C + {}^{13}C$ within the biosphere and the fluxes of total C between the atmosphere and the land biosphere remain unaltered in our simulations ($\phi_{ba}^C = 0$ in (A1) and (A2)). The isotopic composition of carbon in each biospheric pool, on the other hand, is allowed to vary in response to changes in the isotopic composition of the atmospheric CO_2. Thus the mass balances for C and ${}^{13}C$ in biospheric pool i ($I_{b,i}^C$ and $I_{b,i}^{13C}$ in mol C) are

$$\frac{dI_i^C}{dt} = 0 \quad \text{(A3)}$$

$$\frac{dI_i^{13C}}{dt} = \sum_{j \neq i} R_j \alpha_{ji} \phi_{ji}^C - \sum_{i \neq j} R_i \alpha_{ij} \phi_{ij}^C \quad \text{(A4)}$$

where R_γ is the ${}^{13}C/({}^{12}C+{}^{13}C)$ ratio in pool γ and $\alpha_{\gamma\eta}$ and $\phi_{\gamma\eta}^C$ are the fractionation factor and the net carbon flux from pool γ to η (including the atmosphere), respectively. The flux $\phi_{\gamma\eta}^C$ is obviously zero for some combinations (γ, η).

The inventories and fluxes of total C in the land biosphere are taken from Figure 2 of *Siegenthaler and Oeschger* [1987]. The initial biospheric inventories of ${}^{13}C$, on the other hand, are calculated from $I_i^{13C} = R_i I_i^C$, where R_i is the initial ${}^{13}C/({}^{12}C+{}^{13}C)$ ratio in pool i computed from a biospheric $\delta^{13}C$ = -25‰ [*Emanuel et al.*, 1984]. We assume no fractionation between the different biospheric pools, i.e., $\alpha_{ij} = 1$. The exception to this is the photosynthetic incorporation of atmospheric CO_2 into the ground vegetation plus leaves and into wood, for which the fractionation coefficient is equal to 0.982 (from *Tans et al.*, 1993).

In the reference simulation the atmospheric $\delta^{13}C$ changes by 0.2‰–0.3‰ (not shown). The difference between the atmospheric $\delta^{13}C$ simulated with variable and constant ${}^{13}CO_2$ fluxes between the atmosphere and the land biosphere reaches a maximum of 0.06‰. The dilution effect by the land biosphere has thus a significant impact on the atmospheric $\delta^{13}C$ in this simulation.

Appendix B: Approximation of the Variable Thermodynamical Partial Derivatives

For each $i \in \{T, S, \mathrm{DIC}, \mathrm{ALK}\}$ the value of $\partial p\mathrm{CO}_2/\partial i$ between the time steps n and $n+1$ in each surface cell is approximated as

$$\left(\frac{\partial p\mathrm{CO}_2}{\partial i}\right)_{j\neq i} = \frac{p\mathrm{CO}_2(i_{n+1}, \frac{j_n+j_{n+1}}{2}) - p\mathrm{CO}_2(i_n, \frac{j_n+j_{n+1}}{2})}{i_{n+1}-i_n} \quad \text{(B1)}$$

With Δi denoting the change of i from n to $n+1$ the contribution of the variable i to the local $p\mathrm{CO}_2$ change between these two time steps is thus calculated as

$$\left(\frac{\partial p\mathrm{CO}_2}{\partial i}\right)_{j\neq i} \Delta i = p\mathrm{CO}_2(i_{n+1}, \frac{j_n+j_{n+1}}{2}) - p\mathrm{CO}_2(i_n, \frac{j_n+j_{n+1}}{2}) \quad \text{(B2)}$$

Although the latter expression has only a first-order accuracy, it provides a reasonable approximation of the simulated $p\mathrm{CO}_2$ with the time step adopted for the integration of oceanic processes ($\Delta t \approx 3$ weeks).

Acknowledgments. Comments by K. Caldeira, L. Kump, and R. Najjar have improved this paper. We also thank A. Indermühle and J. Schwander for providing information about CO_2 data from the Byrd ice core and total carbon content of Greenland and Antarctic ices, respectively. This study was made possible by the Swiss National Science Foundation and grant BBW 95.0471 from European Projects ENV4-CT95-0131 "Variability of the Glacial and Interglacial Climates and Abrupt Climatic Changes" and ENV4-CT95-0130 "North-South Climatic Connection and Carbon Cycle over the last 250 kyr."

References

Anderson, L. A., and J. L. Sarmiento, Redfield ratios of remineralization determined by nutrient data analysis, *Global Biogeochem. Cycles, 8*, 65–80, 1994.

Anderson, L. A., and J. L. Sarmiento, Global ocean phosphate and oxygen simulations, *Global Biogeochem. Cycles, 9*, 621–636, 1995.

Archer, D., and E. Maier-Reimer, Effect of deep-sea sedimentary calcite preservation on atmospheric CO_2 concentration, *Nature, 367*, 260–263, 1994.

Bard, E., B. Hamelin, M. Arnold, L. Montaggioni, G. Cabioch, G. Faure, and F. Rougerie, Deglacial sea-level record from Tahiti corals and the timing of global meltwater discharge, *Nature, 382*, 241–244, 1996.

Bishop, J. K. B., Regional extremes in particulate matter composition and flux: Effects on the chemistry of the ocean interior, in *Productivity of the Ocean: Present and Past*, edited by W. H. Berger, V. S. Smetacek, and G. Wefer, pp. 117–137, John Wiley, New York, 1989.

Blunier, T., J. Schwander, B. Stauffer, T. Stocker, A. Dällenbach, A. Indermühle, J. Tschumi, J. Chappellaz, D. Raynaud, and J.-M. Barnola, Timing of temperature variations during the last deglaciation in Antarctica and the atmospheric CO_2 increase with respect to the Younger Dryas event, *Geophys. Res. Lett., 24*, 2683–2686, 1997.

Bond, G. C., and R. Lotti, Iceberg discharges into the North Atlantic on millennial time scales during the last glaciation, *Science, 267*, 1005–1010, 1995.

Bond, G., et al., Evidence for massive discharges of icebergs into the North Atlantic Ocean during the last glacial period, *Nature, 360*, 245–249, 1992.

Bond, G., W. S. Broecker, S. J. Johnsen, J. McManus, L. Labeyrie, J. Jouzel, and G. Bonani, Correlations between climate records from North Atlantic sediments and Greenland ice, *Nature, 365*, 143–147, 1993.

Boyle, E. A., Cadmium: Chemical tracer of deepwater paleoceanography, *Paleoceanography, 3*, 471–489, 1988.

Boyle, E. A., and L. Keigwin, Deep circulation of the North Atlantic over the last 200,000 years: Geochemical evidence, *Science, 218*, 784–787, 1982.

Boyle, E. A., and L. D. Keigwin, North Atlantic thermohaline circulation during the past 20,000 years linked to high-latitude surface temperature, *Nature, 330*, 35–40, 1987.

Broecker, W. S., The great ocean conveyor, *Oceanography, 4*, 79–89, 1991.

Broecker, W. S., and E. Maier-Reimer, The influence of air and sea exchange on the carbon isotope distribution in the sea, *Global Biogeochem. Cycles, 6*, 315–320, 1992.

Broecker, W. S., and T.-H. Peng, The role of $CaCO_3$ compensation in the glacial to interglacial atmospheric CO_2 change, *Global Biogeochem. Cycles, 1*, 15–29, 1987.

Broecker, W. S., T.-H. Peng, G. Östlund, and M. Stuiver, The distribution of bomb radiocarbon in the ocean, *J. Geophys. Res., 90*, 6953–6970, 1985.

Broecker, W. S., G. Bond, and M. Klas, A salt oscillator in the glacial Atlantic ?, 1, The concept, *Paleoceanography, 5*, 469–477, 1990.

Broecker, W. S., G. Bond, M. Klas, E. Clark, and J. McManus, Origin of the northern Atlantic's Heinrich events, *Clim. Dyn., 6*, 265–273, 1992.

Bryan, F., High-latitude salinity effects and interhemispheric thermohaline circulations, *Nature, 323*, 301–304, 1986.

Charles, C. D., J. D. Wright, and R. G. Fairbanks, Thermodynamic influences on the marine carbon isotope record, *Paleoceanography, 8*, 691–697, 1993.

Clark, P. U., R. B. Alley, L. D. Keigwin, J. M. Licciardi, S. J. Johnsen, and H. Wang, Origin of the first global meltwater pulse, *Paleoceanography, 11*, 563–577, 1996.

Conkright, M. E., S. Levitus, and T. P. Boyer, *World Ocean Atlas 1994*, vol. 1, *Nutrients*, U.S. Dep. of Comm., Washington, D.C., 1994.

Crowley, T. J., North Atlantic deep water cools the southern hemi-

sphere, *Paleoceanography, 7*, 489–497, 1992.

Curry, W. B., J.-C. Duplessy, L. D. Labeyrie, and N. J. Shackleton, Changes in the distribution of $\delta^{13}C$ of deepwater ΣCO_2 between the last glaciation and the Holocene, *Paleoceanography, 3*, 317–341, 1988.

Dansgaard, W., H. B. Clausen, N. Gundestrup, C. U. Hammer, S. F. Johnsen, P. M. Kristinsdottir, and N. Reeh, A new Greenland deep ice core, *Science, 218*, 1273–1277, 1982.

Dansgaard, W., J. W. C. White, and S. J. Johnsen, The abrupt termination of the Younger Dryas climate event, *Nature, 339*, 532–534, 1989.

Dansgaard, W., et al., Evidence for general instability of past climate from a 250-kyr ice-core record, *Nature, 364*, 218–220, 1993.

Edwards, R. L., W. J. Beck, G. S. Burr, D. J. Donahue, J. M. A. Chappell, A. L. Bloom, E. R. M. Druffel, and F. W. Taylor, A large drop in atmospheric $^{14}C/^{12}C$ and reduced melting in the Younger Dryas, documented with ^{230}Th ages of corals, *Science, 260*, 962–968, 1993.

Emanuel, W. R., G. G. Killough, W. M. Post, and H. H. Shugart, Modelling terrestrial ecosystems in the global carbon cycle with shifts in carbon storage capacity by land-use change, *Ecology, 65*, 970–983, 1984.

Emerson, S., and M. Bender, Carbon fluxes at the sediment-water interface of the deep-sea: Calcium carbonate preservation, *J. Mar. Res., 39*, 139–162, 1981.

Fairbanks, R. G., A 17,000 year glacio-eustatic sea-level record: Influence of glacial melting rates on the Younger Dryas event and deep ocean circulation, *Nature, 342*, 637–642, 1989.

Fairbanks, R. G., The age and origin of the "Younger Dryas climate event" in Greenland ice cores, *Paleoceanography, 5*, 937–948, 1990.

Fanning, A. F., and A. J. Weaver, Temporal-geographical meltwater influences on the North Atlantic conveyor: Implications for the Younger Dryas, *Paleoceanography, 12*, 307–320, 1997.

Farrell, J. W., and W. L. Prell, Climatic change and $CaCO_3$ preservation: An 800,000 year bathymetric reconstruction from the central equatorial Pacific Ocean, *Paleoceanography, 4*, 447–466, 1989.

Fawcett, P. J., A. M. Ågùstsdòttir, R. B. Alley, and C. A. Shuman, The Younger Dryas termination and North Atlantic Deep Water formation: Insights from climate model simulations and Greenland ice cores, *Paleoceanography, 12*, 23–38, 1997.

Froelich, P. N., M. L. Bender, N. A. Luedtke, G. R. Heath, and T. DeVries, The marine phosphorus cycle, *Am. J. Sci., 282*, 474–511, 1982.

Grousset, F. E., L. D. Labeyrie, J. A. Sinko, M. Cremer, G. Bond, J. Duprat, E. Cortijo, and S. Huon, Patterns of ice-rafted detritus in the glacial North Atlantic (40°–55°N), *Paleoceanography, 8*, 175–192, 1993.

Heinrich, H., Origin and consequences of cyclic ice rafting in the Northeast Atlantic Ocean during the past 130,000 years, *Quat. Res., 29*, 142–152, 1988.

Jansen, E., and T. Veum, Evidence for two-step deglaciation and its impact on North Atlantic deep-water circulation, *Nature, 343*, 612–616, 1990.

Johnsen, S. J., H. B. Clausen, W. Dansgaard, K. Fuhrer, N. Gundestrup, C. U. Hammer, P. Iversen, J. Jouzel, B. Stauffer, and J. P. Steffensen, Irregular glacial interstadials recorded in a new Greenland ice core, *Nature, 359*, 311–313, 1992.

Johnsen, S. J., D. Dahl-Jensen, W. Dansgaard, and N. Gundestrup, Greenland palaeotemperatures derived from GRIP bore hole temperature and ice core isotope profiles, *Tellus, Ser. B, 47*, 624–629, 1995.

Keigwin, L. D., and S. J. Lehman, Deep circulation change linked to Heinrich event 1 and Younger Dryas in a middepth North Atlantic core, *Paleoceanography, 9*, 185–194, 1994.

Keigwin, L. D., G. A. Jones, S. J. Lehman, and E. A. Boyle, Deglacial meltwater discharge, North Atlantic deep circulation and abrupt climate change, *J. Geophys. Res., 96*, 16,811–16,826, 1991.

Kroopnick, P. M., The distribution of ^{13}C of TCO_2 in the world oceans, *Deep Sea Res., 32*, 57–84, 1985.

Labeyrie, L., et al., Surface and deep hydrology of the northern Atlantic Ocean during the past 150,000 years, *Philos. Trans. R. Soc. London, 348*, 255–264, 1995.

Legrand, M., and P. Mayewski, Glaciochemistry of polar ice cores: A review, *Rev. Geophys., 35*, 219–243, 1997.

Lehman, S. J., D. G. Wright, and T. F. Stocker, Transport of freshwater into the deep ocean by the conveyor, in *Ice in the Climate System*, edited by W. R. Peltier, *NATO ASI Ser., Ser. I, 12,*, 187–209, 1993.

Leuenberger, M., U. Siegenthaler, and C. C. Langway, Carbon isotope composition of atmospheric CO_2 from an Antarctic ice core, *Nature, 357*, 488–490, 1992.

Lynch-Stieglitz, J., T. F. Stocker, W. S. Broecker, and R. G. Fairbanks, The influence of air-sea interaction on the isotopic composition of organic carbon: Observations and modeling, *Global Biogeochem. Cycles, 9*, 653–665, 1995.

Maier-Reimer, E., and U. Mikolajewicz, Experiments with an OGCM on the cause of the Younger Dryas, *Tech. Rep. 39*, pp. 1–13, Max-Planck-Inst. für Meteorol., Hamburg, Germany, 1989.

Manabe, S., and R. J. Stouffer, Simulation of abrupt climate change induced by freshwater input to the North Atlantic Ocean, *Nature, 378*, 165–167, 1995.

Manabe, S., and R. J. Stouffer, Coupled ocean-atmosphere model response to freshwater input: Comparison to Younger Dryas event, *Paleoceanography, 12*, 321–336, 1997.

Marchal, O., T. F. Stocker, and F. Joos, A latitude-depth, circulation-biogeochemical ocean model for paleoclimate studies: Model development and sensitivities, *Tellus, Ser. B*, in press, 1998.

Mikolajewicz, U., A meltwater induced collapse of the "conveyor belt": Thermohaline circulation and its influence on the distribution of $\delta^{14}C$ and $\delta^{18}O$, *Tech. Rep. 189*, pp. 1–25, Max-Planck-Inst. für Meteorol., Hamburg, Germany, 1996.

Mikolajewicz, U., and E. Maier-Reimer, Mixed boundary conditions in ocean general circulation models and their influence on the stability of the model's conveyor belt, *J. Geophys. Res., 99*, 22,633–22,644, 1994.

Mikolajewicz, U., T. J. Crowley, A. Schiller, and R. Voss, Modelling teleconnections between the North Atlantic and North Pacific during the Younger Dryas, *Nature, 387*, 384–387, 1997.

Mook, W. G., ^{13}C in atmospheric CO_2, *Netherlands J. Sea Res., 20*, 211–223, 1986.

Najjar, R. G., J. L. Sarmiento, and J. R. Toggweiler, Downward transport and fate of organic matter in the ocean: Simulations with a general circulation model, *Global Biogeochem. Cycles, 6*, 45–76, 1992.

Nalewajko, C., and D. R. S. Lean, Phosphorus, in *The Physiological Ecology of Phytoplankton*, edited by

I. Morris, pp. 235–258, Univ. of Calif. Press, Berkeley, 1980.

Neftel, A., H. Oeschger, J. Schwander, B. Stauffer, and R. Zumbrunn, Ice core sample measurements give atmospheric CO_2 content during the past 40,000 yr, *Nature, 295*, 220–223, 1982.

Neftel, A., H. Oeschger, T. Staffelbach, and B. Stauffer, CO_2 record in the Byrd ice core 50,000-5,000 years b.p., *Nature, 331*, 609–611, 1988.

Oeschger, H., J. Beer, U. Siegenthaler, B. Stauffer, W. Dansgaard, and C. C. Langway, Late glacial climate history from ice cores, in *Climate Processes and Climate Sensitivity, Geophys. Monogr. Ser.*, vol. 29, edited by J. E. Hansen and T. Takahashi, pp. 299–306, AGU, Washington, D. C., 1984.

Paillard, D., and L. Labeyrie, Role of the thermohaline circulation in the abrupt warming after Heinrich events, *Nature, 372*, 162–164, 1994.

Rahmstorf, S., Bifurcations of the Atlantic thermohaline circulation in response to changes in the hydrological cycle, *Nature, 378*, 145–149, 1995.

Rau, G. H., T. Takahashi, and D. J. D. Marais, Latitudinal variations in plankton $\delta^{13}C$: Implications for CO_2 and productivity in past oceans, *Nature, 341*, 516–518, 1989.

Sarnthein, M., K. Winn, S. J. A. Jung, J.-C. Duplessy, L. Labeyrie, H. Erlenkeuser, and G. Ganssen, Changes in east Atlantic deepwater circulation over the last 30,000 years: Eight time slice reconstructions, *Paleoceanography, 9*, 209–267, 1994.

Schiller, A., U. Mikolajewicz, and R. Voss, The stability of the North Atlantic thermohaline circulation in a coupled ocean-atmosphere general circulation model, *Clim. Dyn., 13*, 325–347, 1997.

Siegenthaler, U., and H. Oeschger, Biospheric CO_2 emissions during the past 200 years reconstructed by convolution of ice core data, *Tellus, Ser. B, 39*, 140–154, 1987.

Siegenthaler, U., and T. Wenk, Rapid atmospheric CO_2 variations and ocean circulation, *Nature, 308*, 624–626, 1984.

Stauffer, B., et al., Atmospheric CO_2 concentration and millennial-scale climate change during the last glacial period, *Nature, 392*, 59–62, 1998.

Stocker, T. F., and D. G. Wright, Rapid changes in ocean circulation and atmospheric radiocarbon, *Paleoceanography, 11*, 773–796, 1996.

Stocker, T. F., D. G. Wright, and L. A. Mysak, A zonally averaged, coupled ocean-atmosphere model for paleoclimate studies, *J. Clim., 5*, 773–797, 1992a.

Stocker, T. F., D. G. Wright, and W. S. Broecker, The influence of high-latitude surface forcing on the global thermohaline circulation, *Paleoceanography, 7*, 529–541, 1992b.

Stommel, H., Thermohaline convection with two stable regimes of flow, *Tellus, 13*, 224–241, 1961.

Takahashi, T., J. Olafsson, J. G. Goddard, D. W. Chipman, and S. C. Sutherland, Seasonal variation of CO_2 and nutrients in the high-latitude surface oceans: A comparative study, *Global Biogeochem. Cycles, 7*, 843–878, 1993.

Tans, P. P., J. A. Berry, and R. F. Keeling, Oceanic $^{13}C/^{12}C$ observations: A new window on oceanic CO_2 uptake, *Global Biogeochem. Cycles, 7*, 353–368, 1993.

Veum, T., E. Jansen, M. Arnold, I. Beyer, and J.-C. Duplessy, Water mass exchange between the North Atlantic and the Norwegian Sea during the past 28,000 years, *Nature, 356*, 783–785, 1992.

Vidal, L., L. Labeyrie, E. Cortijo, M. Arnold, J.-C. Duplessy, E. Michel, S. Becqué, and T. C. E. Van Weering, Evidence for changes in the North Atlantic Deep Water linked to meltwater surges during the Heinrich events, *Earth Planet. Sci. Lett., 146*, 13–27, 1997.

Wright, D. G., and T. F. Stocker, A zonally averaged ocean model for the thermohaline circulation, I, Model development and flow dynamics, *J. Phys. Oceanogr., 21*, 1713–1724, 1991.

Wright, D. G., and T. F. Stocker, Sensitivities of a zonally averaged global ocean circulation model, *J. Geophys. Res., 97*, 12,707–12,730, 1992.

Wright, D. G., and T. F. Stocker, Younger Dryas experiments, in *Ice in the Climate System*, edited by W. R. Peltier, *NATO ASI Ser., Ser. I, 12*, 395–416, 1993.

Zahn, R., J. Schönfeld, H.-R. Kudrass, M.-H. Park, H. Erlenkeuser, and P. Grootes, Thermohaline instability in the North Atlantic during meltwater events: Stable isotope and ice-rafted detritus records from Core so75-26kl, portuguese margin, *Paleoceanography, 12*, 696–710, 1997.

F. Joos, O. Marchal, and T. F. Stocker, Climate and Environmental Physics, Physics Institute, University of Bern, Sidlerstraße. 5, CH-3012 Bern, Switzerland. (e-mail: marchal@climate.unibe.ch)

(Received November 18, 1997;
revised February 25, 1998;
accepted March 1, 1998.)